AFRL-AFOSR-UK-TR-2010-0017

Spectroscopy Measurements on Ablation Testing In High Enthalpy Plasma Flows

Olivier P Chazot

Von Karman Institute for Fluid Dynamics (VKI)
72 Chaussee de Waterloo
Rhode-Saint-Genese, Belgium B-1640

EOARD GRANT 08-3069

November 2010

Final Report for 01 August 2008 to 01 August 2010

Air Force Research Laboratory
Air Force Office of Scientific Research
European Office of Aerospace Research and Development
Unit 4515 Box 14, APO AE 09421

REPORT DOCUMENTATION PAGE

Form Approved OMB No. 0704-0188

1. REPORT DATE *(DD-MM-YYYY)*	2. REPORT TYPE	3. DATES COVERED *(From – To)*
04 November 2010	Final Report	01 August 2008 – 01 August 2010

4. TITLE AND SUBTITLE

Spectroscopy Measurements on Ablation Testing In High Enthalpy Plasma Flows

5a. CONTRACT NUMBER

FA8655-08-1-3069

5b. GRANT NUMBER

Grant 08-3069

5c. PROGRAM ELEMENT NUMBER

61102F

6. AUTHOR(S)

Professor Olivier Chazot

5d. PROJECT NUMBER

5d. TASK NUMBER

5e. WORK UNIT NUMBER

7. PERFORMING ORGANIZATION NAME(S) AND ADDRESS(ES)

Von Karman Institute for Fluid Dynamics (VKI)
72 Chaussee de Waterloo
Rhode-Saint-Genese B-1640
Belgium

8. PERFORMING ORGANIZATION REPORT NUMBER

Grant 08-3069

9. SPONSORING/MONITORING AGENCY NAME(S) AND ADDRESS(ES)

EOARD
Unit 4515 BOX 14
APO AE 09421

10. SPONSOR/MONITOR'S ACRONYM(S)

AFRL/AFOSR/RSW (EOARD)

11. SPONSOR/MONITOR'S REPORT NUMBER(S)

AFRL-AFOSR-UK-TR-2010-0017

12. DISTRIBUTION/AVAILABILITY STATEMENT

Approved for public release; distribution is unlimited.

13. SUPPLEMENTARY NOTES

14. ABSTRACT

The objective of this work is to develop the capability of testing and characterization of ablative materials exposed to high enthalpy plasma flows including both classical and spectroscopic based measurement techniques. Two different ablative material specimens, a newly developed carbon resin composite ablator (MONA, Lockheed Martin) and a cork compound (AMORIM Cork composites), were selected to perform the measurements.

A comprehensive setup of measurement techniques was applied to the Plasmatron facility (chapter 3) to determine and characterize temperature evolution inside and at the surface of the sample as well as the recession rate. Further, the chemical composition of the free-stream and the surrounding gas layer in front of the sample during the ablation process was determined using emission spectroscopy.

The obtained results are presented in chapter 5, which depicts the degradation of the samples due to ablation (mass loss & surface recession), different temperature measurements (surface & inside) and spectroscopic results (freestream & ablation). A final conclusion of the whole test campaign is made in chapter 6 summarizing the results obtained.

15. SUBJECT TERMS

EOARD, Thermal Protection & Control, Plasma Aerodynamic, Hypersonic Flow

16. SECURITY CLASSIFICATION OF:			17. LIMITATION OF ABSTRACT	18, NUMBER OF PAGES	19a. NAME OF RESPONSIBLE PERSON
a. REPORT	b. ABSTRACT	c. THIS PAGE			Gregg Abate
UNCLAS	UNCLAS	UNCLAS	SAR	47	19b. TELEPHONE NUMBER *(Include area code)* +44 (0)1895 616021

von Karman Institute for Fluid Dynamics
Aeronautics / Aerospace Department

Chaussée de Waterloo, 72
B - 1640 Rhode Saint Genèse
Belgium

Contract Report: VKI CR 2010-18

Internal Ref.: 10/VKI/AR/OC/ARR0810/FR

Spectroscopy Measurements on Ablation Testing In High Enthalpy Plasma Flows (Grant 83069)

Final Report

von Karman Institute for Fluid Dynamics

Von Karman Institute for Fluid Dynamics		**CLASSIFICATION** 1. Unclassified 2. Industry 3. Restricted 4. Confidential	☐ ☐ ☐ ☐	**CATEGORY** 1. For approval 2. For review 3. Other	☐ ☐ ☐
		CONFIGURATION			
		Controlled	☐	Not Controlled	☐
Program number	Program	Contract number ARR0810		Work package number	

TITLE:

Spectroscopy Measurements on Ablation Testing In High Enthalpy Plasma Flows

Final Report

AUTHOR(S):

C. O. Asma, B. Helber, T. Magin, O. Chazot

ISSUE. Date: 27th Oct, 2010 Issue 1 Rev. 0.	Internal Reference Number 10/VKI/AR/OC/ARR0810/FR	Number of pages: 45 Number of included annexes: 0

SUMMARY:

This final technical report presents the progress performed on the contract work entitled "Spectroscopy Measurements on Ablation Testing In High Enthalpy Plasma Flows".

HOST SYSTEM	**HARDWARE EQUIPMENT.** Nature: PC	**MEDIA.** Nature & Type: Identification:	**SOFTWARE.** Name: Microsoft Word
KEY WORDS		**LANGUAGE CODE** **ENG**	**APPROVAL.**
			Section: High Speed Aerodynamics
			Department: Aeronautics/Aerospace

Von Karman Institute for Fluid Dynamics	DOCUMENT REVISIONS TRACEABILITY SHEET DOCUMENT 10/VKI/AR/OC/ARR0810/FR		
Version	**Date:**	**Status:**	**No. of pages:**
Title: **Author:** **Features:**			
Version	**Date:**	**Status:**	**No. of pages:**
Title: **Author:** **Features:**			
Version	**Date:**	**Status:**	**No. of pages:**
Title: **Author:** **Features:**			

1 INTRODUCTION 5
2 LITERATURE SURVEY 8
3 VKI PLASMA FACILITIES AND MEASUREMENT PROBES 10
3.1 VKI PLASMATRON FACILITY 10
3.2 HEAT FLUX MEASUREMENT DEVICES 11
3.2.1 THE HIGH HEAT FLUX PROBE 12
3.2.2 CURRENT PROBLEMS WITH THE HIGH HEAT FLUX PROBE 13
3.2.3 ENHANCEMENT OF THE HIGH HEAT FLUX PROBE 14
3.3 THE ABLATIVE MATERIAL SAMPLES 15
3.4 THERMOCOUPLES 16
3.5 INFRARED THERMOGRAPHY 17
3.5.1 INFRARED CAMERA 18
3.5.2 PYROMETER 18
3.5.3 BROADBAND RADIOMETER 18
3.6 PRESSURE PROBE 19
3.7 EMISSION SPECTROSCOPY 19
3.7.1 EMISSION SPECTROSCOPY SYSTEM 19
3.7.2 SPECIES DUE TO ABLATION 21
3.8 HIGH SPEED CAMERA 22
3.9 OPERATING CONDITIONS 23
4 LOCAL HEAT TRANSFER SIMULATION 25
5 MEASUREMENT RESULTS AND DISCUSSIONS 26
5.1 MASS LOSS AND RECESSION 26
5.2 SURFACE AND INSIDE TEMPERATURE MEASUREMENTS 27
5.3 EMISSION SPECTROSCOPY MEASUREMENTS 32
5.3.1 FREESTREAM CHARACTERIZATION NITROGEN AND AIR 32
5.3.2 MONA ABLATION SPECTRA IN NITROGEN PLASMA 34
5.3.3 MONA ABLATION SPECTRA IN AIR PLASMA 36
5.3.4 CORK ABLATION SPECTRA IN AIR PLASMA 37
6 CONCLUSION 40
7 RECOMMENDATIONS FOR FUTURE WORK 42
ACKNOWLEDGEMENTS 43
REFERENCES 44

1 INTRODUCTION

The most critical component for the success of any space mission of vehicles entering a planetary atmosphere is the thermal protection system (TPS). It has to withstand the high temperature environment of the hypersonic gas flow. This causes the kinetic and potential energy of the vehicle being converted into thermal energy through a strong shock wave, which is heating the gas to high temperatures (T ~ 10,000K at 10 km/s velocity). After the successful manned missions to the Moon and many probe entries into the atmosphere of outer planets, the next challenges for the space agencies include bringing back samples to Earth and continuing the manned exploration program, which aims to send human beings to Mars and bring them home safely. The European Space Agency (ESA) is also developing an Advanced Re-entry Vehicle (ARV) for crew and cargo transportation from the International Space Station. This uses the heritage of the Atmospheric Re-entry Demonstrator (Figure 1-1), which flew successfully in 1998, as well as the work carried out in the period 1998-2002 on the Crew Return Vehicle for the ISS and associated technologies

Figure 1-1: Artistic view of Atmospheric Re-entry Demonstrator (ARD)

Although many achievements in rocket science have been made since Apollo, prediction of the heat-flux to the surface of the spacecraft remains an imperfect science, and inaccuracies in these predictions can be fatal for the crew or the success of robotic missions. Engineers resort to safety factors to determine the heat shield thickness, at the expense of reduced mass of embarked payload. Difficulty is enhanced for Earth re-entries at velocities higher than 10

km/s, typical of the new missions of ESA and NASA, where ablative materials are used instead of reusable materials for the TPS.

Nowadays ablators are made out of light-weight materials like phenolic compounds whose physico-chemical processes are very complex and not well understood up to this date. Hence, thorough experimental analysis in ground test facilities and improved numerical modeling are required for an accurate prediction of the heat flux. These ablative TPS allow heat rejection through various complex physico-chemical mechanisms leading to material removal through pyrolysis and ablation shown in Fig 1-2. Pyrolysis is the mechanism of outgassing products, due to sublimation of the phenolic resin fillers, diffusing into the boundary layer after motion through the porous material and leaving a low density carbon. The pyrolysis gases are transported out of the material by diffusion and convection through the pores. During this transfer, their chemical composition evolves as their temperature increases and as they mix with air that diffuses into the pores of the material from the boundary layer. Finally, the exhaust gases exit into the boundary layer providing a further barrier for the heat exchange but might undergo additional chemical reactions, creating highly radiating species which can increase the radiative heat flux.

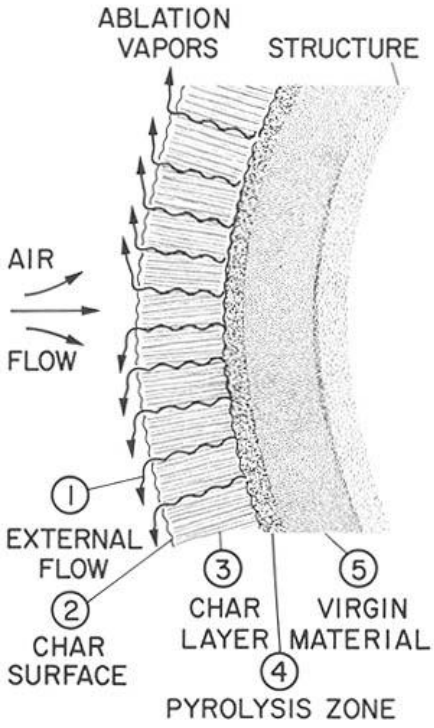

Figure 1-2: Process of pyrolysis and ablation of a charring ablator

Ablation is the degradation of the char layer, composed of fibrous preform and the carbonized resin, promoted by heterogeneous chemical reactions (oxidation, nitridation), phase change (sublimation) and mechanical erosion (shear stresses and spallation). During this transformation, charred material is directly removed from the ablator what leads to recession of the surface. Further, the char layer acts like a blockage for oxygen diffusion from the boundary layer to the virgin material inside.

Hence, ablative materials are designed to slowly burn away in a predicted manner, so that heat energy can be transformed and carried away from the spacecraft by the gases generated by the ablative process; while the remaining solid material insulates the vehicle from superheated gases.

Thorough understanding of the material response of low density carbon/resin composite ablators is crucial to ensure safety of the astronauts and payload for the future space missions. Thus, experimental research is necessary for advancement of the prediction tools used for the TPS design of tomorrow's space vehicles and planetary probes.

The objective of this work is to develop the capability of testing and characterization of ablative materials exposed to high enthalpy plasma flows including both classical and spectroscopic based measurement techniques. Two different ablative material specimens, a newly developed carbon resin composite ablator (MONA, Lockheed Martin) and a cork compound (AMORIM Cork composites), were selected to perform the measurements.

A comprehensive setup of measurement techniques was applied to the Plasmatron facility (chapter 3) to determine and characterize temperature evolution inside and at the surface of the sample as well as the recession rate. Further, the chemical composition of the free-stream and the surrounding gas layer in front of the sample during the ablation process was determined using emission spectroscopy.

The obtained results are presented in chapter 5, which depicts the degradation of the samples due to ablation (mass loss & surface recession), different temperature measurements (surface & inside) and spectroscopic results (freestream & ablation).

A final conclusion of the whole test campaign is made in chapter 6 summarizing the results obtained.

2 LITERATURE SURVEY

There is some helpful information of the recent studies which provide updated information about ablative material physics, modelling and associated measurement techniques. Some of them are repeated in the following sections.

Laub et al[2], explains the difference between reusable and ablative TPS materials and their application areas. They give a short chronologic history of ablative TPS materials used so far for NASA entry missions. Guthrie et al[3], explains the mechanism of TPS materials and gives information about different types of TPS. Chen and Milos[4] have investigated shape change simulations for charring ablators. The governing equations include both energy conservation and a three-component decomposition model with a moving grid.

Gordeev A. N.[5] explains the characteristics of IPG series Plasmatron, their applications for re-entry simulation and thermal protection material testing. Thömel et al[6], focuses on the reliability of the Local Heat Transfer Simulation (LHTS) methodology which is used to determine the catalycity effect in order to select a proper TPS material. The numerical and experimental tools that are used to simulate the flow in the VKI Plasmatron within the LHTS are briefly explained. In order to implement the LHTS, an experiment, including heat flux and pressure measurement, is carried out and then the flow inside the facility is simulated numerically. The experimental tool (facility) that is used to measure the heat flux and pressure is the VKI Plasmatron. The numerical tools that are used for flow simulation are the Inductively Coupled Plasma Code (ICP Code), a stagnation line boundary layer solver for chemical non-equilibrium boundary layer (NEBOULA), and the rebuilding code which is called CERBOULA. As a result of the uncertainty analysis, they found that the uncertainty in terms of catalycity is mostly due to the heat flux measurements[6].

Gülhan A.[7] gives information about the non-intrusive temperature measurement techniques namely the pyrometry and IR thermography and their application at high temperatures. In another study, Gülhan A.[8] explains the fundamentals of heat transfer

measurement techniques in high enthalpy flows. Kurtz et al[9], explains the theoretical basics and measurement principle of two non-intrusive temperature measurement techniques: Pyrometry and emission spectroscopy; and describes the experimental setup for emission spectroscopic measurements, the intensity and wavelength calibration procedures and the Abel inversion which are important factors for evaluating the measured data.

Bottin et al[10], gives information about the VKI Plasmatron facility, the measurements which are carried out in this facility and the measurement devices. They give the description of heat flux probe and Pitot probe and their working principle. They also give the heat flux; total-static pressure; and total enthalpy distribution which are procured at four different conditions namely [8 g/s, 250 kW, 15hPa], [8 g/s, 150 kW, 15 hPa], [16 g/s, 250 kW, 15 hPa] and [8 g/s, 250 kW, 75hPa] to observe the effect of each parameter. Vancrayenest and Fletcher[11], performed an ablation test using graphite as a test material and investigated the interaction of ablation products and outgassing species with the plasma flow. The tests are carried out in the Minitorch inductively coupled plasma facility at lower enthalpy conditions. The limited capability of the Minitorch for ablation studies proven by the test results, forced the researchers perform the tests in the VKI Plasmatron with a greater enthalpy range. In another study, Vancrayenest and Fletcher[12] uses emission spectroscopy for graphite ablation test in the VKI Plasmatron. The tests are performed at different static pressures of 50, 100 and 200 mbar for nitrogen and air plasmas with a mass flow rate of 16 g/s. Dynamic pressure and heat flux are measured at the same time with a combined calorimeter. Yang [13], analyzes the problems with the current high heat flux probe which are summarized in Figure 1. He designs and manufactures a film cooling pipe which is shown in Figure 2 to make the heat flux probe resistant to high heat flux conditions. The pipe is designed to cool the probe holder and is mounted directly on the leading edge of the probe holder. The study of Orsini[14] presents the design of a new calorimeter to be used in the plasma wind tunnel for high enthalpy flows. He compares the new and standard calorimeter in terms of measured heat flux by performing experiments in Plasmatron facility at different static pressure values changing in the range 15 -200 mbar and power values changing from 100 kW to 200 kW.

3 VKI PLASMA FACILITIES and MEASUREMENT PROBES

This chapter describes the experimental facility used for all the measurements and introduces the measurement techniques applied to each experiment. We review the different measurement techniques, intrusive and non-intrusive. A more thorough description can be found in the references cited in the text. The ablative test sample on which the investigation is carried out is also presented.

3.1 VKI PLASMATRON FACILITY

Plasma wind tunnels are used for development and qualification of radiation, thermal protection systems and re-entry measurement devices; and validation of numerical codes for re-entry prediction. The VKI Plasmatron facility which is shown in Figure 3.1 is the most powerful facility of this kind in the world and offers a unique opportunity to test ablative materials associated with a collection of measurement techniques. The Plasmatron facility is an inductively-coupled plasma (ICP) wind tunnel equipped with 1.2 MW, 400 kHz, high frequency generator and has two interchangeable torches which have 80 and 160 mm diameters. ICP is a type of plasma source in which the energy is supplied by electrical currents which are produced by electromagnetic induction that is by time varying magnetic fields. It creates high purity plasma flow with heat fluxes up to 10 MW/m^2. Since there is no contact with plasma formation and electrodes, the plasma jet is not contaminated by any vaporized electrode material that can cause catalysis on the probe holder. The tunnel is operated with argon, air and CO_2 plasmas.

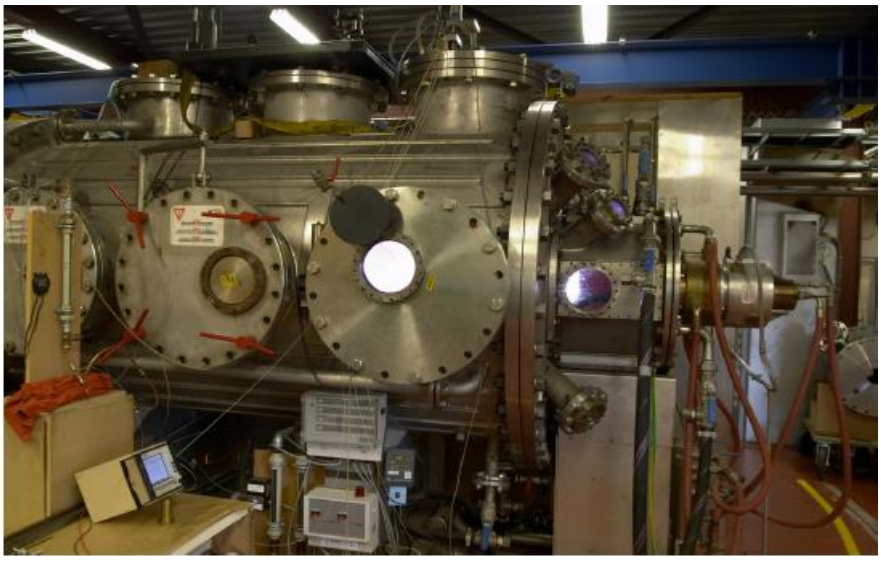

Figure 3-1: VKI Plasmatron Facility

3.2 HEAT FLUX MEASUREMENT DEVICES

Heat flux measurements are carried out using a calorimetric probe by measuring the heat flux to a relatively cold surface. The water-cooled calorimeter is located at the center of the high heat flux probe. Two thermocouples are located on both inlet and outlet water pipes of the calorimeter to measure the temperature difference which is needed to calculate the heat flux by using the Equation 3.1.

Generally water is used for cooling the probe. The heat flux onto the front surface of the probe is obtained by measuring the temperature difference between the inflow and outflow of the cooling water and its mass flow. Substituting these parameters into equation given below leads to calculation of the heat flux which is carried off by the cooling water.

$$\dot{q} = \frac{\dot{m} C_p \left(T_{out} - T_{in} \right)}{S} \qquad (3.1)$$

Where, S is the front surface area of the probe [m^2], m is the mass flow rate [g/s], C_p is the specific heat capacity of the cooling water [kJ kg^{-1} K^{-1}]. T_{out} and T_{in} are the water temperature at respectively outlet and inlet of the sensing element [K]. A typical heat flux measurement curve is given in Figure 3.2. The probe is injected at the 101.5th second and taken away at121.5th second. After a certain time the heat flux value becomes steady state and the data is taken after achieving this steady state condition. In this figure it is achieved after approximately 118.5th seconds.

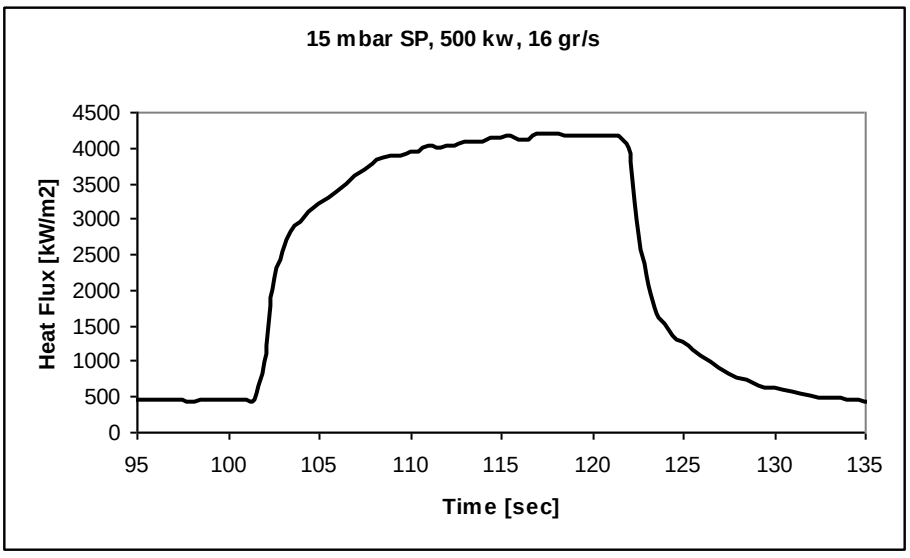

Figure 3-2: Typical behavior of a heat flux curve

During heat flux measurements one must keep in mind that the mass flow rate of the water should be high enough to avoid nucleate boiling and low enough to have higher temperature difference and thus lower uncertainty.

3.2.1 The High Heat Flux Probe

The high heat flux probe used in the Plasmatron facility is a hemispherical probe of 50 mm in diameter made of brass with a copper head. It has cooling loops to protect from high heating. This probe is shown in Figure 3.3.

For the heat flux measurement the material of the probe itself has an important effect since the heat transfer may vary depending on the catalycity of the material. In addition, the surface temperature of the probe may affect the recombination rate and its emission coefficient. Copper is mostly used material for heat flux probes owing to its relatively high catalytic efficiency.

Figure 3-3: The standard (left) and hemispherical (right) heat flux probes

During the measurements, the heat flux probe is first located at 445 mm away from the torch exit; but then it is located at 320 mm which is two times the diameter of the torch as

shown in Figure 3.4. As stated in the study of Kolesnikov[15], under typical subsonic test conditions the optimum distance Z_m between the model and the exit is estimated as $D_m < Z_m < 2D_c$.

In this region:

- flow perturbations induced by the model do not reach the torch
- the flow past the model exposed in the central part of the jet is close to axisymmetric
- the high stability of the free jet parameters
- the uniform heat loading on the sample face
- the stagnation point heat flux and the surface temperature of the sample are reproducible
- the flow enthalpy and velocity along the free-jet axis decrease only slightly

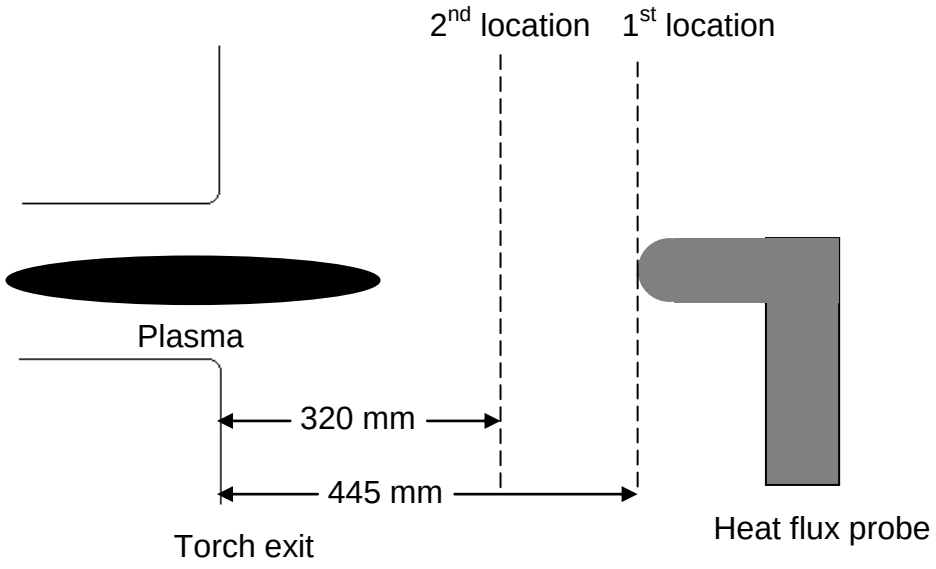

Figure 3-4: Heat flux probe location

3.2.2 Current Problems with the High Heat Flux Probe

The standard heat flux probes can not stand to measure high heat fluxes up to 10 MW/m^2 due to overheating problems. For example the rubber O-ring that joins the probe to the probe holder melts during measurements and causes leakages within the cooling loop and this causes some critical parts to be subjected to overheating. Also, this water leakage causes the pressure raise in the freestream. The problems with the heat flux probe can be summarized as the melting of the O-ring, failure of the cooling loops, nucleate boiling inside the

calorimeter and burning of the surface of the probe[13]. The critical parts that are subjected to huge temperature are shown Figure 3.5.

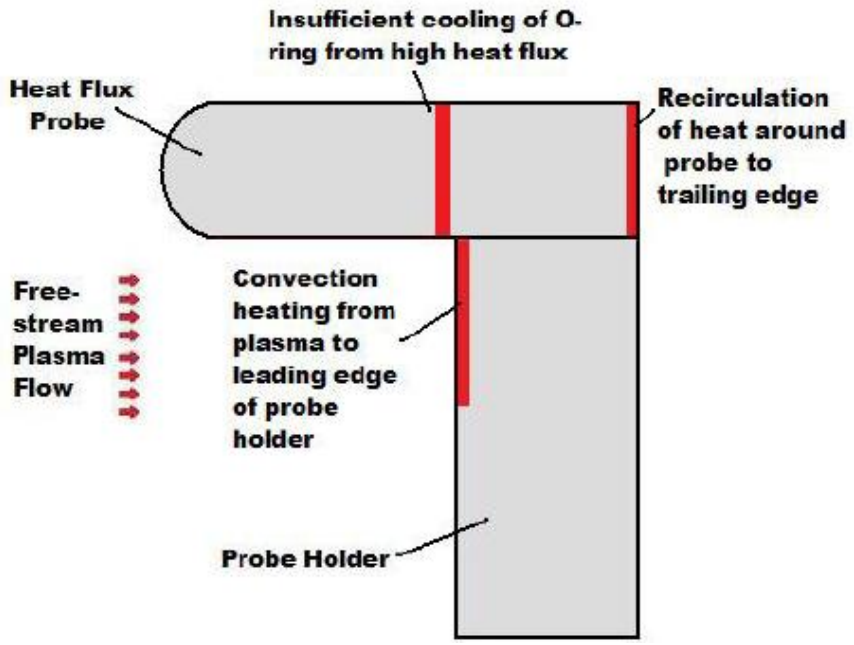

Figure 3-5: Critical regions on the heat flux probe[13]

3.2.3 Enhancement of the High Heat Flux Probe

Before starting the heat flux measurements the heat flux probe enhancement is needed to avoid the problems mentioned in the previous section. To achieve high heat flux, a spiral cooling pipe made of copper which is shown in Figure 3.6 is mounted on the probe holder to protect the body from huge heating. Also a Teflon ring PTFE (Poly Tetra Fluora Ethylene) which is a kind of ablative material is located on the probe holder for the same aim. Also a cork block is put in front of the probe holder to prevent burning of the critical parts.

Figure 3-6: The hemispherical heat flux probe with the cooling spiral and ablative ring

3.3 THE ABLATIVE MATERIAL SAMPLES

In this study, the behaviour of two different ablative materials is examined at different heat fluxes. A carbon-resin composite ablator (MONA), made of a carbonic matrix filled with resin, and a cork composite in a phenolic compound are selected to perform the ablation tests. The models and the dimensions of the models are given in Figure 3-7. The ablative samples are mounted on the probe holder and installed with temperature surveillance as shown in Figure 3-7.

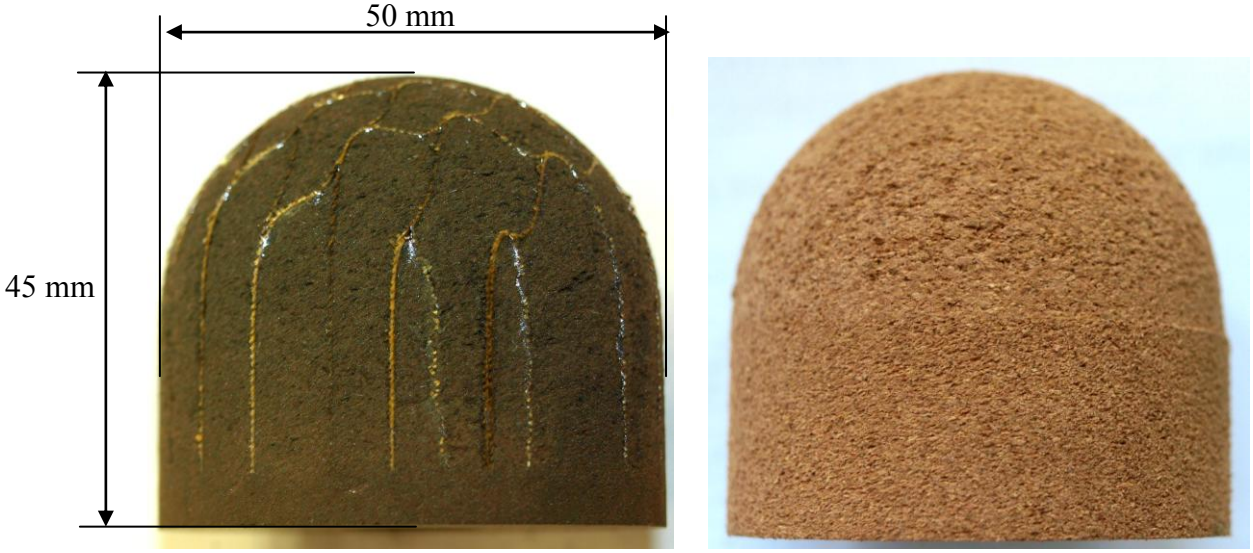

Figure 3-7: MONA (left) and cork (right) ablative samples before testing

The new type of ablators developed today are light-weight, low dense composite materials made up of carbon fibres impregnated with a phenolic resin or as cork in a

compound. These materials show a different and more complex behaviour than rather dense ablators, which were extensively examined and used a lot in the past. For these new ablators, the process of ablation is not only restricted to the surface but can also occur in depth. If oxygen is able to diffuse further into the porous material, this is expected to lead rather to a volumetric ablation than to a pure material decomposition at the surface. This calls for a more complex experimental characterisation of the material and makes it more difficult to model its response properly.

Several publications (Ahn et al[22]) pointed out the major area of ambiguity as the state of the pyrolysis gases leaving the char zone, which depend only on temperature and not on the surrounding gas. Sublimation gases are formed above 100°C temperature by the complex mechanisms of outgassing of organic products like the phenolic resin fillers, which are then diffusing into the boundary layer after motion by convection and diffusion through the material leading to a pressure increase. Within the process of pyrolysis a char layer is formed, composed of the carbonized resin and the remaining carbonic fibres. The degradation of this char layer is then promoted chemically through oxidation and nitridation, phase changes (sublimation), and mechanical erosion (spallation). Possible volumetric ablation arises now from the ability of oxygen to diffuse into the porous material, as mentioned by Lachaud et al.[23], leading to a decrease of density by oxidation.

3.4 THERMOCOUPLES

A thermocouple is a junction between two different metals that produces a voltage related to a temperature difference. The relationship between the temperature difference (ΔT) and the output voltage (V) of a thermocouple is linear.

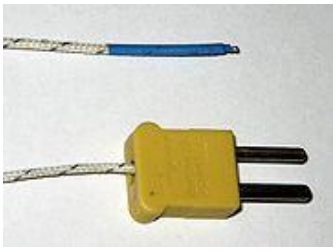

Figure 3-8: K-type thermocouple

K type (chromel–alumel) thermocouple as shown in Figure 3-8 is the most common general purpose thermocouple. It is inexpensive and available in a wide variety of probes. They are available in the −200 °C to +1300 °C range as given in Table 3.1.

Type	K (Chromel-Alumel)
Range of Linearity	-200 to1300^{o}C
Sensitivity	0.04 mV/ ^{o}C

Table 3-1: Characteristics of K-type thermocouple

The thermocouples are fastened to the plastic pipes with a copper tube to measure the inlet and outlet temperature of the calorimeter.

During ablation tests, two thermocouples; one of them at 10 mm the other at 20 mm away from the stagnation point, are located on the ablative material sample.

3.5 InfraRed THERMOGRAPHY

Surface temperature measurement is a topic of great concern in high enthalpy and hypersonic flows. Therefore non intrusive measurement techniques are developed to be used for the models which have chemical reactions between the solid and gas phases at high temperatures since other temperature measurement devices such as thermocouples have limited application in such environments. Both IR thermography and pyrometer are non intrusive surface temperature measurement techniques.

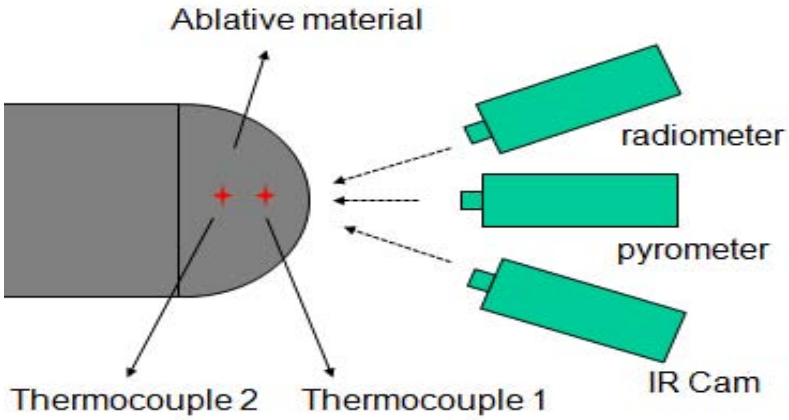

Figure 3-9: Temperature measurements on the test sample

3.5.1 InfraRed Camera

The used Infrared Camera (ThermaCAM SC^{TM} 3000) produces images of invisible infrared or heat radiation and provides precise non contact temperature measurements. It detects radiation in the infrared region and converts it into an electronic signal, which is then processed to produce a thermal image on a video monitor and perform temperature calculations. When the temperature distribution is obtained, one can use it to determine the local heat transfer coefficients.

3.5.2 Pyrometer

Further surface temperature measurements are carried out with a sampling rate of fs = 1Hz using a two-colour Raytek Marathon MR1S-C pyrometer (0.75 − 1.1μm), with a temperature range from 1000°C to 3000°C. It measures the infrared radiation of a high temperature material at two different narrow wavelengths. The temperature is calculated by building the ratio of the radiation intensities. The main assumption is that the emissivity of the surface is the same at those two wavelengths. The advantages of the procedure are:

- the emission coefficient of the work piece does not have to be known
- smoke and dirt do not affect the measurement
- non-intrusive method
- the measurement object can be smaller than the spot of the pyrometer

Surface temperature is an important parameter for ablation and recession since it has an important effect on oxidation and sublimation of the char layer. Therefore, during the tests the surface temperature of the front face of the model is measured by the pyrometer.

3.5.3 Broadband Radiometer

The infrared radiometer Heitronics KT 19.XX is used as an additional front surface temperature information source and it is located in front of a KRS-5 window. The radiometer functions in the wavelength range of 0.6 to 40 μm, and provides as output the integrated thermal radiation over this spectrum within a temperature range of 0 to 3000ºC. The radiometer is calibrated using a black body radiation source to take the transmissivity of the KRS-5 window into account. The acquisition rate is 1 Hz. The raw radiometer data assumes an emissivity of 1.

3.6 PRESSURE PROBE

It is possible to measure the dynamic and total stagnation pressure of the plasma flow with a Pitot probe by connecting them to a total pressure gauge outside of the vacuum tank.

3.7 EMISSION SPECTROSCOPY

Emission is the process by which the energy of a photon is released by another entity, for example, by an atom whose electrons make a transition between two electronic energy levels. The emitted energy is in the form of a photon. The emission spectrum is the set of light (electromagnetic radiation) frequencies emitted by substances after they have been excited with various forms of energy, most commonly heat or electrical.

Emission Spectroscopy is used to determine atomic and molecular density and temperature distribution in the plasma flow. It corresponds to a line of sight measurement which has to be processed to obtain local data. The light energy emitted by an element of the plasma flow is passed by a polychromator and a photoelectric multipler as the detector to the electronics and processed in the microprocessor. Finally, the content of each element present is calculated by system software.

Instrumentation of the emission spectroscopy is composed of a light collection system, a spectrograph (polychromator) or monochromator, and a photo detector. A monochromator is an optical device that transmits a mechanically selectable narrow band of wavelengths of light or other radiation chosen from a wider range of wavelengths available at the input. A device that can produce monochromatic light has many uses in science and in optics because many optical characteristics of a material are dependent on color. Although there are a number of useful ways to produce pure colors, there are not so many other ways to easily select any pure color in a wide range.

3.7.1 Emission Spectroscopy System

An overview of the VKI Plasmatron facility with the optical diagnostic bench applied can be found in Figure 3-10. The light emitted by the plasma and chemical reactions was collected through a variable aperture and focused by a converging lens (300mm focal length, LA4579) onto the entry of a 600μm diameter optical fibre. This lead to the HR-4000 spectrometer, which covers a broad spectrum (200 − 1100nm), making it suitable to rapidly

determine radiating transitions of atoms and main molecular bands. Further, a comparable high acquisition rate (here: fs = 2Hz) providing real time acquisition spectra makes it ideal for ablation testing. The entrance slit aperture of about 5 mm lead to a typical resolution of approximately 0.6nm (depending slightly on the spectral range). An integration time of the acquisition system of t_I = 5ms was used with an average of av = 10, what still lead to saturation of the spectra for the higher heat flux tests.

The optical diagnostic bench (aperture, lens, fibre) was mounted on a movable holding system, which enables vertical and horizontal movements to be able to place the line of sight to the desired position. This was checked and adjusted before each experiment using a laser beam, which was sent through the optics and located ahead of the initial stagnation point of the sample. The optical system was then fixed with an initial distance from the sample of around d = 1 − 2mm and not moved during the whole experiment. The line of sight of the optical probing did not follow the recessing surface of the sample and emission decay was observed during the experiment as the material is ablated. Calibration of the whole system in relative intensity (Figure 3-11), consisting of the light collection mechanism and spectrometer efficiencies, was performed with a deuterium lamp in the UV range (< 400nm) and with a ribbon tungsten lamp in the visible.

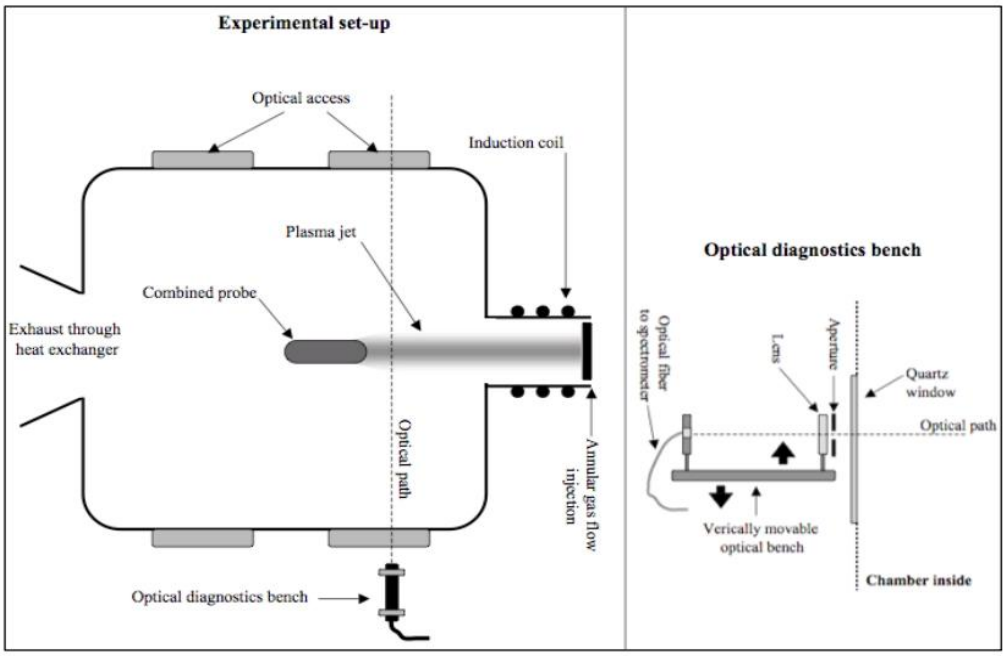

Figure 3-10: Schematic view of the VKI Plasmatron with optical diagnostic bench for emission spectroscopy

Measurements with ablative samples were performed in air as well as pure nitrogen flow to constrict chemical reactions in the absence of oxygen.

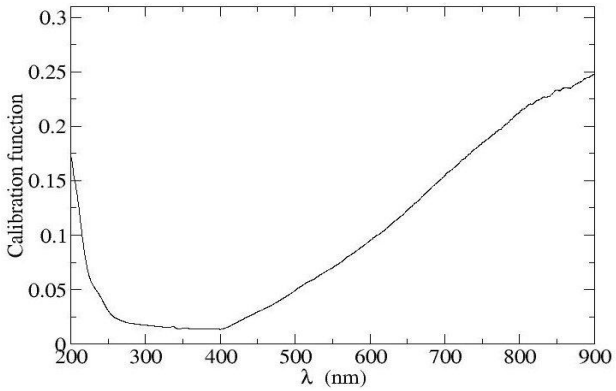

Figure 3-11: Calibration function in the UV and visible spectral region

The repeatability of the measurements has been checked, insuring the relative uncertainty on the total integrated emission of the radiative signature to be less than 10%.

3.7.2 Species due to ablation

A key issue in an ablation study is to include all relevant chemical species such as the flow field species, the gaseous species injected by the ablator, the interaction between the flow field species and the injected species.

The initial species are N_2, O_2 since the working gas is air. As the flow passes through the shock wave, due to dissociation and reactions N, O, NO are formed. Figure 3-12shows the number of species for different missions.

Generally the emission spectroscopy at the subsonic air flows is dominated by the emission of molecules NO, N_2 and N_2^+ in the UV region. Molecular emission of N_2 and atomic O and N are visible to the near infrared wavelength region. O atom is visible at 777 nm. The species injected by the ablator are carbonic structures as C, C_2, C_3, if sublimation is reached, as well as O and H due to sublimation of the resin. Due to interaction between the flow field and injected species, CN, CO and CO_2 are formed. The relevant species are N_2, N_2^+, CN, O and N. (Radiation of O_2, NO and CO is important in UV region, but below spectral range).

The CN violet system dominates the spectrum with a maximum close to 388 nm ($\Delta v=0$) and high intensities for sequences $\Delta\upsilon = \pm 1$. (CN violet system is dominant radiating species over the range from 350-450 nm). For higher wavelengths CN red system dominates the spectrum. CN red emission occurs in the range 600-900 nm. CN violet is visible in UV, whereas CN red is visible in Infrared[12].

For atoms there is no vibration and rotation, there is only transition level whereas there are transition, vibration and rotation levels for molecules.

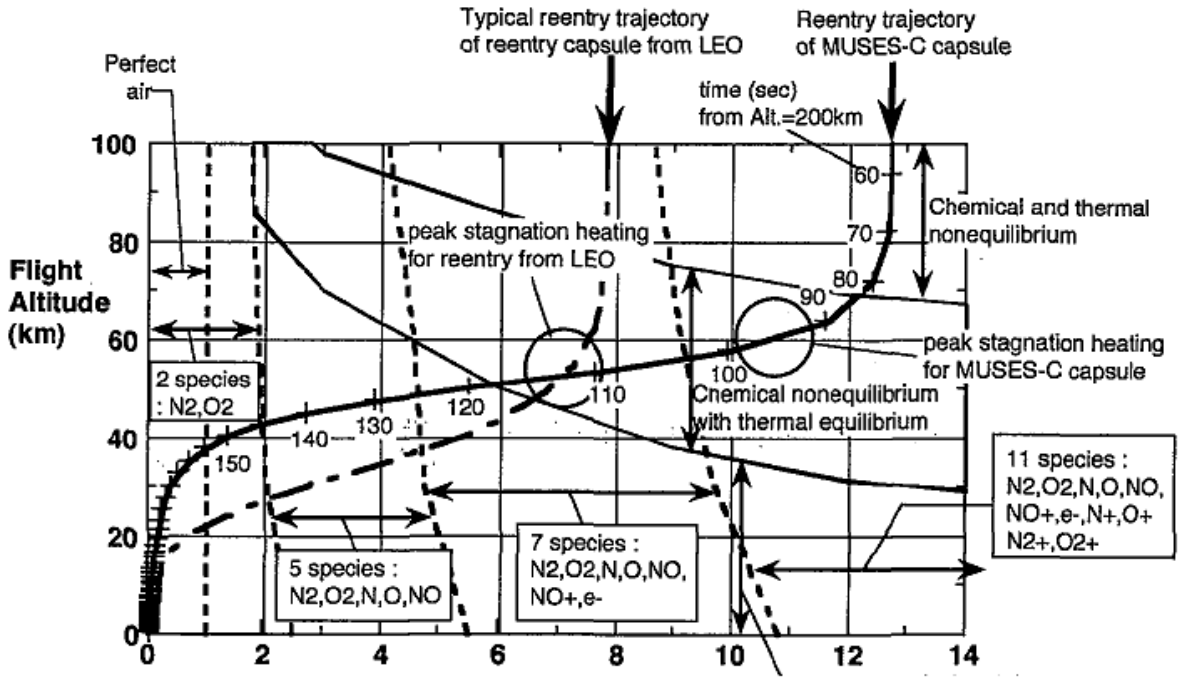

Figure 3-12: Chemical Non-equilibrium viscous shock layer analysis[18]

3.8 High Speed Camera

The Vision Research Phantom 7.1 CMOS high-speed camera (HSC) provides the possibility to use very short exposure times (minimum: 2µs) to capture an image with a varying sampling frequency. As a preferably high resolution was needed for the processing of the HSC as well as a recording time equal to the test time, the sampling frequency had to be adjusted and was set to $f_{s,HSC}$ = 12fps with an exposure time of 5µs. A 200mm telephoto lens was used with an aperture between 16 − 22 depending on the heat flux. The obtained images

were then post-processed depending on the favoured results. High heat fluxes exceeding 3MW/m² lead mostly to saturation of the 8 bit CCD sensor although the smallest aperture was used. Calibration of the resulting images was made using the known dimensions of the test sample to obtain the correlation pixel:millimeter.

Figure 3-13 shows all measurement techniques applied inside the Plasmatron test chamber.

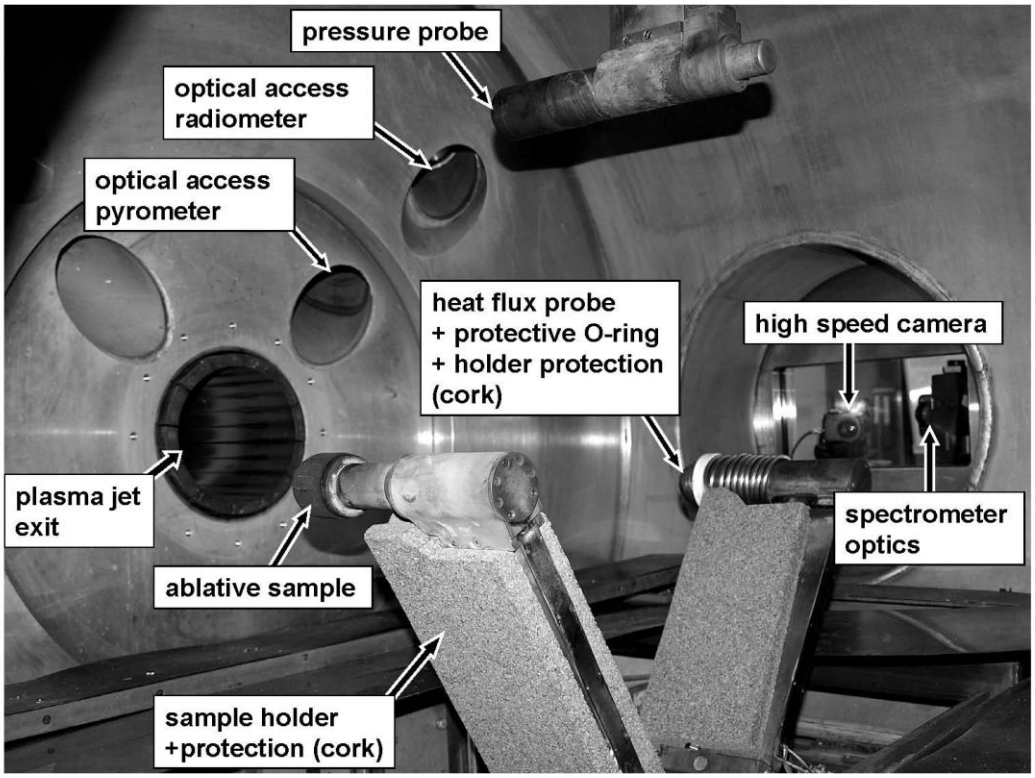

Figure 3-13: Experimental setup in the Plasmatron facility with free-stream characterisation techniques (heat flux probe, pressure probe) and measurement techniques for ablation characterisation

3.9 OPERATING CONDITIONS

Air is the gas that is selected to be used as a working gas. The mass flow rate of air, static pressure and the power of the plasma generator are given in Table3-2.

Mass flow rate [g/s]	16
Static Pressure [mbar]	100
Heat Flux [kW/m^2]	1000 – 3000

Table3-2: The operating conditions for the experiments

The first tests are carried out on graphite samples to make sure the proper functionality of the intended measurement techniques. Then, the experimental campaign was performed using carbon resin composite (MONA) and cork-based ablative materials.

4 LOCAL HEAT TRANSFER SIMULATION

The high temperature can cause the dissociation of molecules into atoms and ionization of atoms into ions. These dissociated species can recombine at the surface. The property at the surface that promotes such phenomena is called catalycity. An increase in catalycity implies that more species are releasing their formation energy at the wall of the vehicle increasing the heat transfer.

The aim of the LHTS methodology is to duplicate representative flight conditions in ground based facilities. It allows to test and to determine the catalycity in order to choose more suitable materials for TPS. It is based on the results of experiments and numerical simulations of plasma flows in ICP plasma facilities to determine the chemical surface properties such as recombination rate of dissociated species near a catalytic surface.

First, an experiment is conducted in a plasma facility that creates a plasma jet impinging on a probe with a known catalycity. In air flow, a copper calorimeter is used since it is known to be highly catalytic. In addition to heat flux, pitot pressure measurements are taken.

Secondly, the numerical simulation of the flow inside the facility is carried out for the same ambient conditions (ambient pressure and mass flow rate) and boundary layer characterizing values (Non dimensional parameters-NDP) are determined.

In the chamber, it is assumed that the thermochemical equilibrium takes place and the flow simulated using the ICP code [10].

It allows defining the boundary layer that develops around the probe which is characterized by the boundary layer thickness, perpendicular velocity at the boundary layer edge v_e and tangential derivative of the tangential velocity component at the boundary layer edge, $(du/dx)_e$. These quantities help to define non-dimensional parameters that will serve as input to the non-equilibrium boundary layer code presented below.

A rebuilding code called CERBOULA incorporates a stagnation line boundary layer solver NEBOULA for chemical non-equilibrium assuming a finite boundary layer thickness which is suitable for low Reynolds number free stream[6]. It computes the free stream enthalpy at stagnation point for a given set of experimental conditions. It can also determine the catalytic properties, through an identification process, by comparing numerical results with measurement data from tested TPS [10].

5 MEASUREMENT RESULTS AND DISCUSSIONS

5.1 Mass loss and recession

The mass loss of the tested samples was obtained by simply weighing them before and after testing with a Kern EW150-3M balance (1*mg* precision). For recession measurements a 0.1*mm* precise calliper rule was used for pre- and post-test evaluation. Results can be found in Table 5-1. Whilst for the MONA samples clearly a recession of the surface due to ablation could be measured, depending on the heat flux and exposure time, for the cork samples this was rather difficult. As the test sample expanded during the test, what is most likely due to the high-heating and pressure increase inside the material due to pyrolysis gases, a direct analysis of the recession by pre- and post-test evaluation was not possible. Hence, there are demands for the development of other methods to be able to give an appropriate recession analysis about the lost material by char removal.

sample	***test gas*** [-]	***heat flux*** [MW/m²]	***test time*** [s]	***recession*** [mm]	***mass loss*** [g]
MONA	air	1.0	100	7.00	4.15
MONA		3.0	30	4.50	6.19
MONA	N_2	1.0	100	1.30	4.24
MONA		3.0	30	1.29	5.12
Cork	air	1.0	30	-	7.65
Cork		3.0	30	-	13.3

Table 5-1: Recession and mass loss for different ablative samples and test conditions

From the results the increase in mass loss related to a higher heat flux can directly be seen. As the temperature inside the material increases with a higher heat flux the process of pyrolysis is enhanced, leading to a stronger charring process whilst releasing more O and H atoms. Besides, the effect of oxygen with using air as test gas can be depicted as the recession in air test cases is much higher than in nitrogen. Oxidation leads to a fast degradation of the char layer (leading to CO and CO_2) whilst in nitrogen mostly mechanical erosion and nitridation lead to removal of char from the surface.

For the MONA sample, recession estimation was also possible to be performed by means of a high speed camera. With this, the recessing surface was able to be tracked and applying contour detection at the beginning and the end of the tests enabled to estimate the changing surface line.

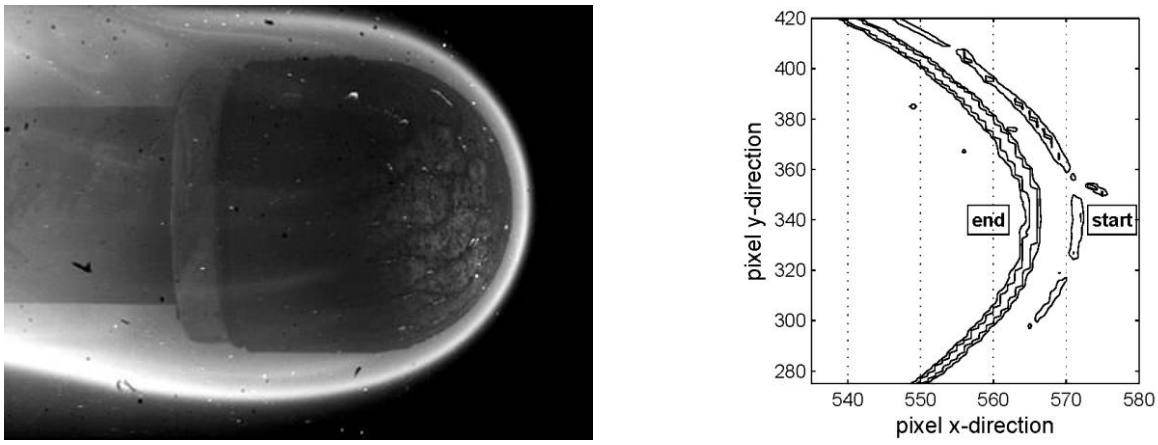

Figure 5-1: HSC snap-shot during ablation test and contour plot of processed images indicating test start and test end

High speed camera imaging was not applied to all test cases, but the obtained data is consistent with recession measurements done by using the calliper rule. Furthermore, with this new promising technique the evaluation of recession speed during ablation tests is able to be performed.

5.2 Surface and Inside Temperature Measurements

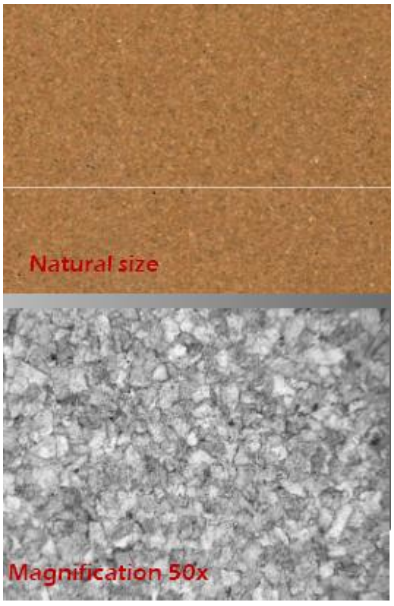

Figure 5-2:Close-up and magnified views of Amorim P50

Figure 5-3: Amorim P50 samples before (left) and after (right) test

Several Amorim P50 cork composite ablative thermal protection materials are tested at 1 MW/m^2 and 3 MW/m^2 heat flux conditions in the Plasmatron facility. The heat flux is measured by a water cooled (350K) copper calorimeter, which is highly catalytic with respect

to oxygen and nitrogen recombinations. The mass flow rate of air is kept at 16 g/s and the static pressure of the test chamber at 100 mbar. The Amorim P50 is a high strength cork composition made with 0.5 to 1 mm cork granule and a special binder for high heat resistance. It has a specific heat of 2018 J/(kg K) within a temperature range of 38 to 316 ºC (100 to 600 F) and a thermal conductivity of 0.0820 W/(K m) at 38 ºC (100 F) and 0.0822 W/m/K at 260 ºC (500 F). Figure 5-2 shows a close-up view and the magnified view of the Amorim P50 sheet. The P50 samples tested in the Plasmatron facility are 50mm diameter hemispherical samples, as shown in Figure 5-2 (front view), before and after exposure to the air plasma flow.

Two type K thermocouples are utilized to measure the temperature inside the test sample 10 mm and 20 mm behind the stagnation point, as shown in Figure 5-4. These measurements are very useful in determining the thermal efficiency of the ablative material, where the inner (back) temperature of the sample is required to be low despite the high front surface temperature. Figure 5-5 presents typical results from the two thermocouples utilized for the condition of 3 MW/m^2 heat flux. Following the ignition of the Plasmatron facility, the sample starts heating, not because of ablation or exposure to plasma flow, but simply because it is in the close vicinity of a high temperature high enthalpy plasma flow. The Plasmatron facility is stopped after 30 seconds of exposure. The 30 second exposure to plasma is shown in Figure 5-5 by the pink rectangular section, where no change in the slope of the temperature curve is observed, indicating that the observed temperature rise is due to heating from the side, not from the stagnation point. The increase in the inner temperature value is more significant after the 30 second exposure to plasma flow. This shows that the heat experienced by the stagnation point of the sample is transferred to the inner regions by a significant time delay, which is a very promising property of the tested thermal protection material.

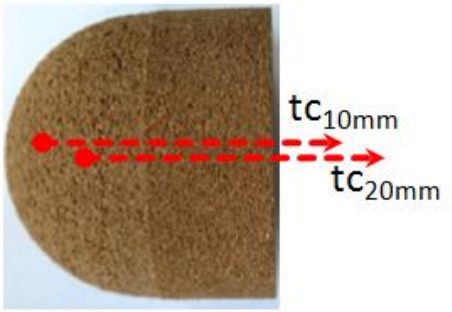

Figure 5-4: **Location of the two thermocouples measuring the temperature 10 mm and 20 mm inside the sample**

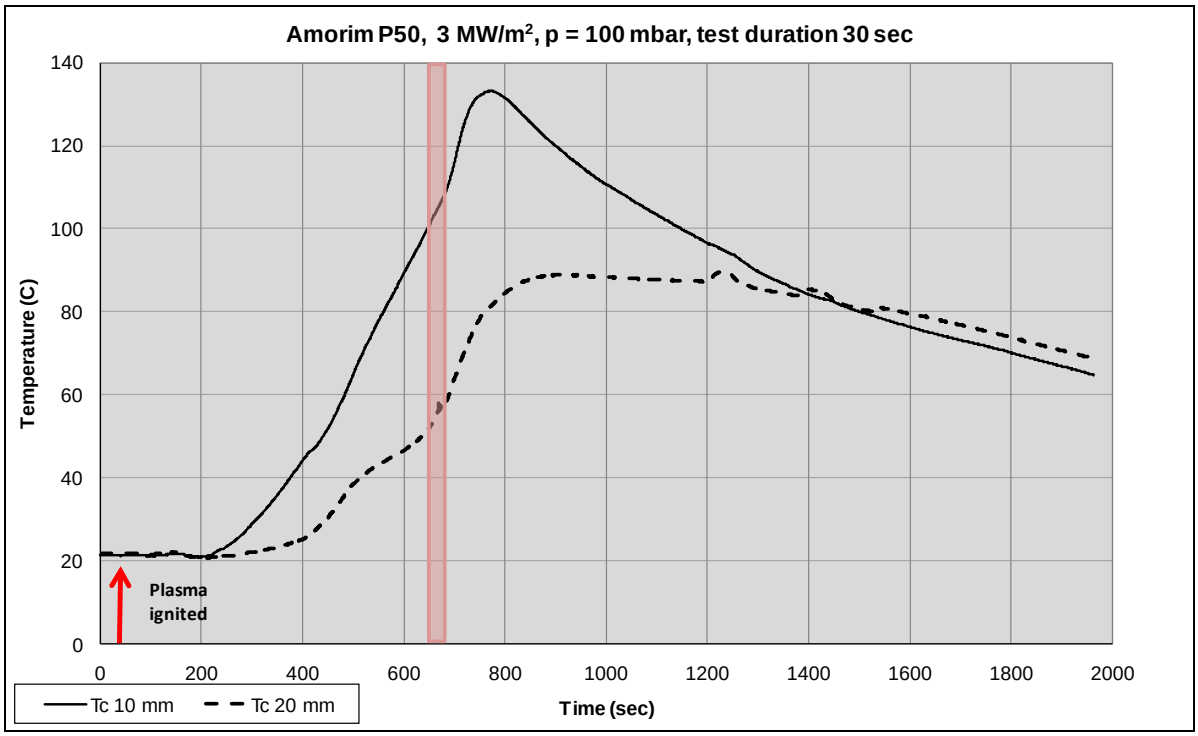

Figure 5-5: **Temperature change inside the sample before, during (pink) and after exposure to plasma flow**

Although the thermocouples read between 100 ºC and 130 ºC maximum inside the sample during and after the exposure to plasma flow at 3 MW/m^2 heat flux, the front surface temperature recorded by the two-colour pyrometer and the other infrared thermography devices are much higher. Figure 5-6 and Figure 5-7 present the front face temperature values as a function of time during the 30 seconds exposure to plasma flow, as observed by the two colour pyrometer, the infrared camera and the radiometer, for 1 MW/m^2 and 3 MW/m^2 incident heat flux conditions, respectively. The average front surface temperature is 1650 ºC for the 1 MW/m^2 heat flux condition and it is 2300 ºC for the 3 MW/m^2 heat flux condition, as recorded by the calibrated two-colour pyrometer.

The front face temperatures measured by the two-colour pyrometer, the infrared camera and the radiometer are plotted as a function of time in Figure 5-6 and Figure 5-7. For both plots, t = 0 corresponds to the injection of the ablative sample into the plasma flow and the test duration is 30 seconds. For both cases, the pyrometer values do not need any correction as the pyrometer is calibrated for the test conditions and it is theoretically independent of the emissivity of the test sample. However, the infrared camera and the radiometer readings need to be corrected taking the emissivity into account. The infrared

values presented in Figure 5-6 (for 1 MW/m^2 heat flux condition) are corrected assuming a factor of 0.66 for the transmissivity of the ZnSe (τ) window multiplied by the emissivity (ε) of the test sample (where the radiation intensity is $I = \sigma.\tau.\varepsilon.T^4$). On the other hand, a factor of 0.64 is employed to correct the infrared camera results for the case of 3 MW/m^2 presented in Figure 5-7. The transmissivity of the ZnSe window employed in front of the infrared camera is in the order of 0.95 for the wavelength range of 8 – 9 μm, as presented in Figure 5-8. Considering a transmissivity of 0.95 for the ZnSe window, the emissivity measured by the infrared camera corresponds to 0.70 for the 1 MW/m2 heat flux case (1650 C temperature) and to 0.67 for the 3 MW/m2 heat flux case (2300 C temperature). A similar analysis can be performed by comparing the results of the radiometer to the results of the pyrometer, employing the methodology proposed by [9]. In accordance with this methodology, the emissivity is calculated to be 0.73 (±0.08) for the 1 MW/m2 heat flux case (1650 C temperature), and to be 0.68 (±0.04) for the 3 MW/m2 heat flux case (2300 C temperature). These values are in agreement with those obtained from the comparison of the infrared camera results with the pyrometer results. In the plots of Figure 5-6 and Figure 5-7, both uncorrected and corrected radiometer results (by the mentioned emissivity values) are presented. It should be noted that the radiometer emissivity values do not need any correction for the transmissivity of the KRS-5 window, as this is already taken into consideration during the calibration of the radiometer.

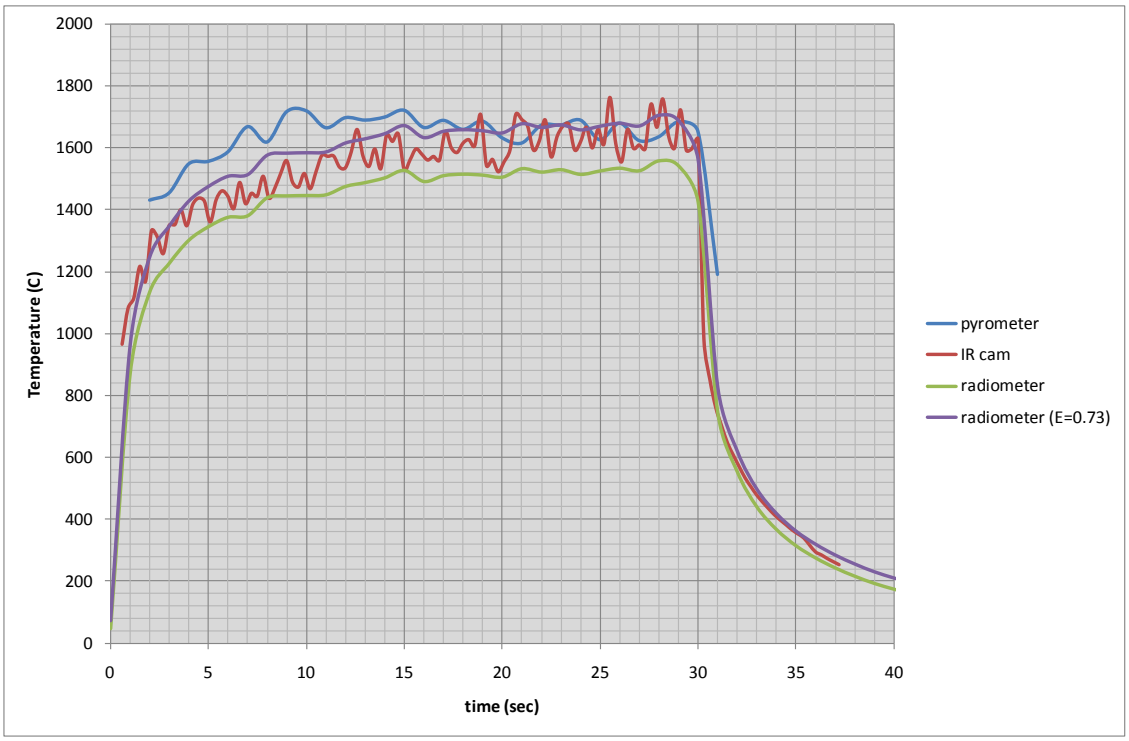

Figure 5-6: **Front face temperatures for the test at 1 MW/m^2 heat flux**

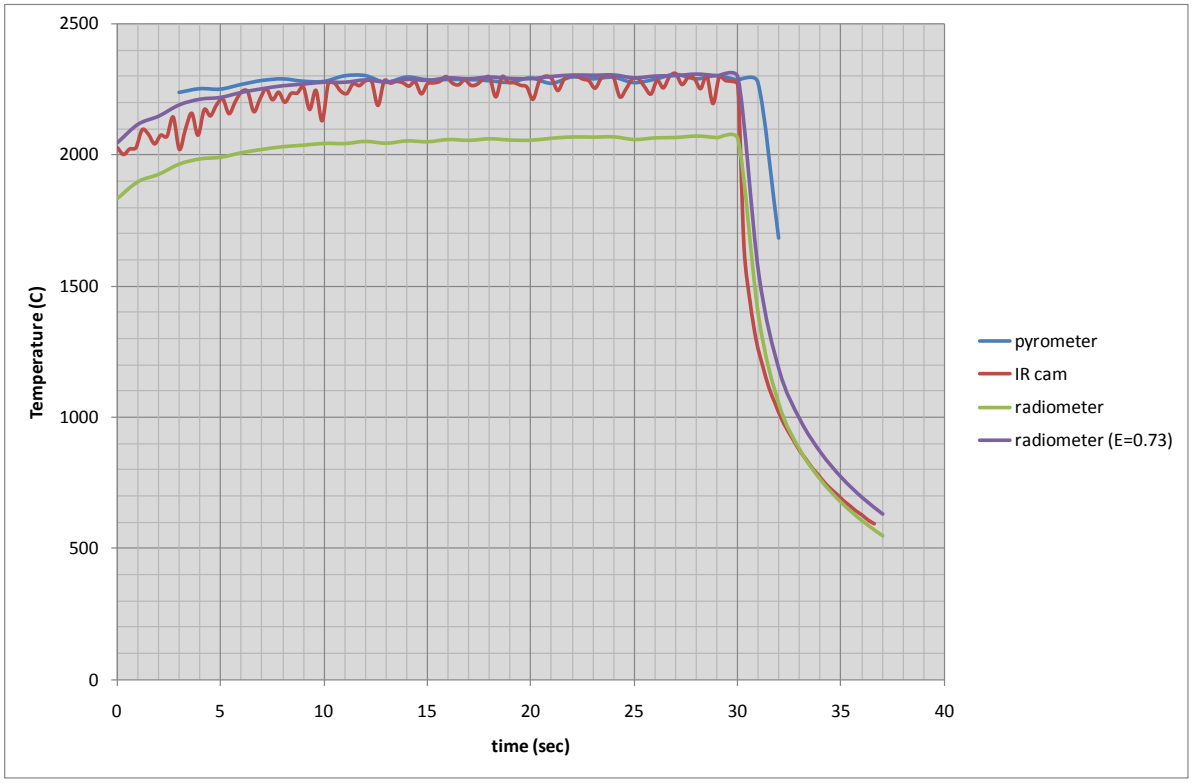

Figure 5-7: **Front face temperatures for the test at 3 MW/m^2 heat flux**

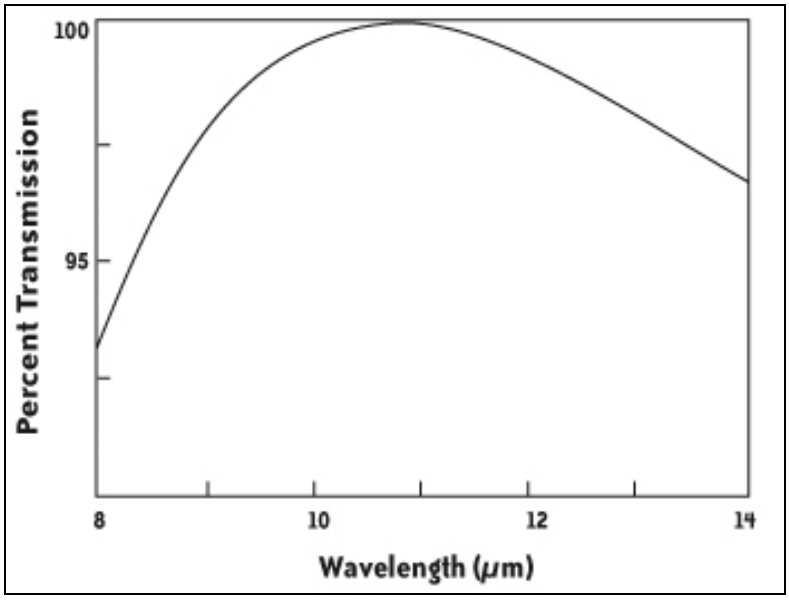

Figure 5-8: **Transmissivity of the ZnSe window**

Figure 5-9: Back view (left) and side view (right) of test samples before (only side view) and after test

Finally, it is interesting to observe the relatively very low temperature values inside the samples measured by thermocouples and compared to front face temperatures. This is believed to be due to conversion of the incident heat flux into ablation and sublimation of the ablative material. The ablation mechanism takes place in a very controlled manner and at a certain temperature, avoiding the heat wave to penetrate deeper into the material. An evidence for this assumption can be seen in Figure 5-9, where the back view of a tested sample is shown. The black char layer (ablated section) penetrates into the material following a very uniform pattern.

5.3 Emission Spectroscopy Measurements

5.3.1 Freestream characterization nitrogen and air

Before injection of the sample into the test gas, measurements of the pure plasma flow were recorded by the spectrometer. With that, assumptions can be made on the composition and thermodynamic state of the test gas by comparing different spectra, shown in Figure 5-10 for different heat fluxes. As expected, for nitrogen test gas the spectrum is mainly dominated by emission of molecular N_2, the N_2^+ system and also atomic nitrogen for higher

temperatures. The first negative system of N_2^+ (1-) is the main radiating species in the range of 296-470 nm in the UV region (<400 nm) as well as the first positive system of N_2(1+) in the visible region (400-750 nm). For increasing heat flux atomic nitrogen is also visible with the usual triplet at 742, 744 and 746 nm as well as further atomic lines in the near infrared (NIR, 750-1400 nm). Additionally, a higher concentration of N_2^+ (1-) is observed for the higher heat flux of 3MW/m² identified with a higher intensity. No atomic oxygen, especially the 777 nm triplet, is visible in both cases speaking for a pure nitrogen test flow without leakage in the test chamber as oxygen would start to dissociate before N_2 dissociation. Besides, the noisy signal for low intensities can be recognized which was induced by subtracting the optical background of the signal response.

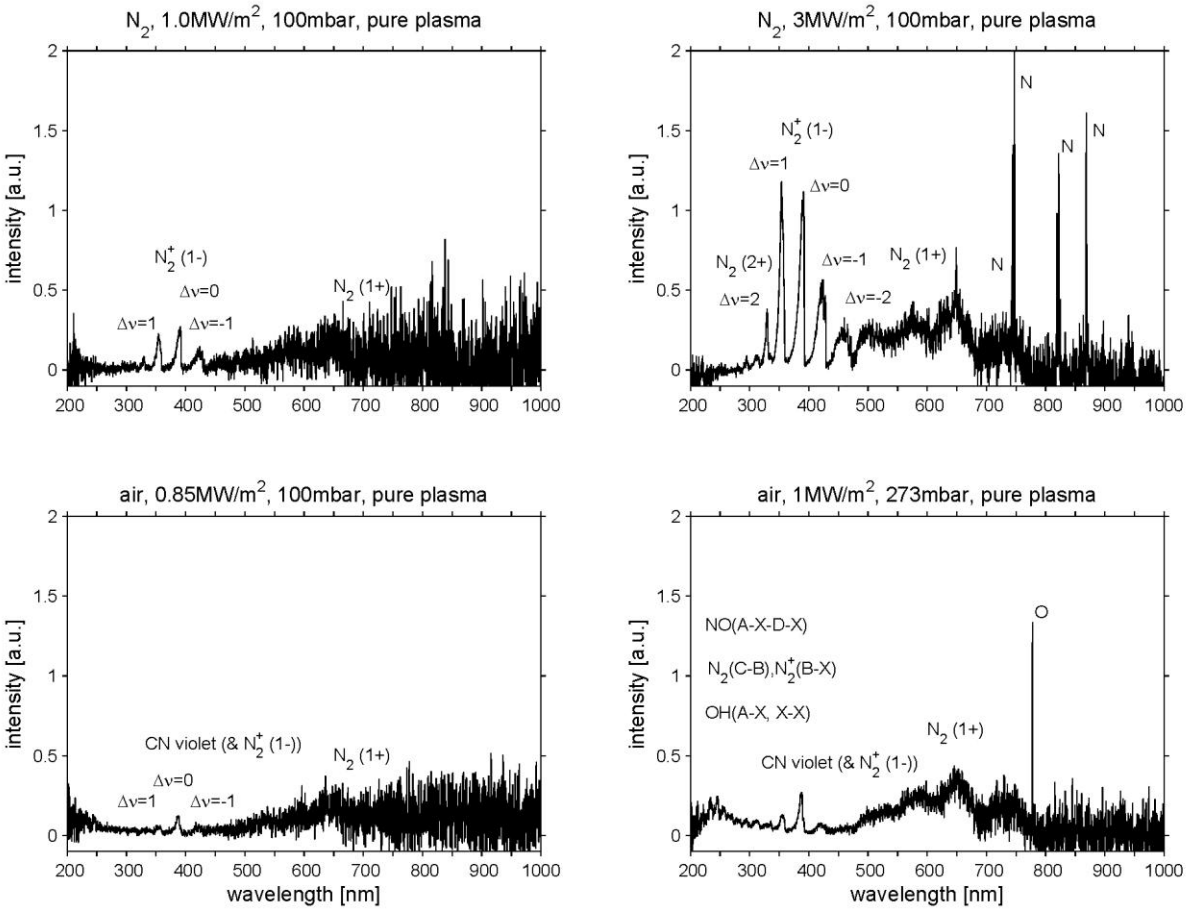

Figure 5-10: Emission spectra of pure nitrogen and air plasma flows for different heat fluxes, p_s=100 mbar

This is different compared to the air test gas before sample injection also shown in Figure 5-10. Here, N2$^+$ (1-) is still apparent but mainly overlapped by the CN violet system in the 350-450 nm region, both having a very similar spectrum. The first positive system of N_2 is again present and especially for the higher pressure/higher heat flux test case for air test gas the 777 nm atomic oxygen triplet is visible. Further, in the UV region below 350 nm

emissions of NO (A-X to D-X transition) were captured with other possible contributors, for instance overlapping transitions of OH (A-X, X-X).

5.3.2 MONA ablation spectra in nitrogen plasma

In nitrogen test gas, no oxidation of the char at the surface is able to occur, hence, no CO formation has to be regarded, except for the amounts of oxygen coming from pyrolysis, limiting the number of possible reactions. Figure 5-11 depicts spectra ahead of the tested sample in nitrogen flow for different points in time after sample injection and two heat fluxes (0.85MW/m² (a) and 1.0MW/m² (b)).

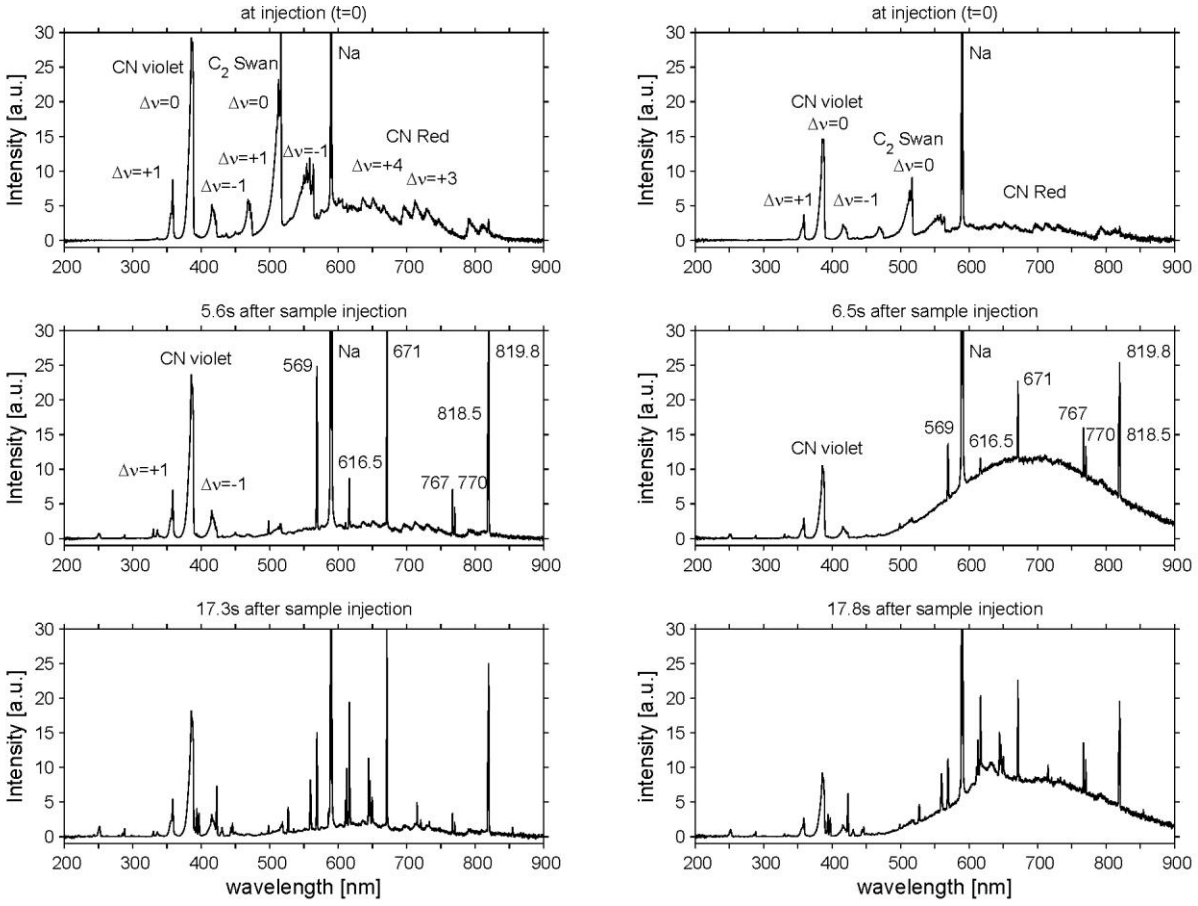

(a) ***(b)***

Figure 5-11: Emission spectra ahead of the ablating MONA sample in nitrogen test gas at different times after injection for 0.85MW/m² (a) and 1.0MW/m², 100mbar (b)

Unlike the free-stream spectra shown before, a strong CN violet system is now visible below 450nm resulting from carbon induced by the sample and the absence of oxygen. Care has to be taken for overlapping sequences, especially Δν = 0, -1 of CN violet are very similar

to N_2^+ (1-). Additionally, right after injection of the sample CN red emission is visible in the long wavelength part above 600 nm

The third strong system taking part at the start-up of the ablation process in nitrogen is found to be C_2 represented by the C_2 Swan system emission with the $\Delta v = 0$ band head at 516.5 nm. No atomic lines are present in the spectrum taken at sample injection except for a very strong emitting line at 589 nm which is most likely assignable to the sodium (Na) double rule at 588.99 nm and 589.59 nm, respectively, which are called D_1 and D_2 lines. Sodium might be one of the products comprised by the phenolic composition or could be due to impurities during the manufacturing process. However, this highly radiating sodium line is present throughout all test cases in nitrogen, air and argon.

Mostly the same behaviour can be assigned to the test case with slightly higher heat flux presenting again carbon nitride and molecular carbon as main contributors of radiation beside the strong atomic line of sodium.

Time resolved spectra of the ablation process were taken with a frequency of f_s =2 Hz. Therefore, an evaluation over time of the obtained spectra can be made showing also results of points in time at t=5.6s and t=17.3s. Whilst the CN violet system only shows a slight decrease during the time sequence presented, a big difference can be identified regarding molecular carbon as the C_2 Swan system disappears almost completely within the first 5.6s. Further, in the same instance multiple atomic contributors emerge from the ablation process resulting in strong emission lines at 569nm, 616.5nm, 671.2nm, 766.9nm, 770.4nm and a doublet at 818.6/819.8nm in a wide wavelength range. At this point the reader is referred to the NIST database[21].

Comparing the observations made above with the higher heat flux test, the same evolution regarding the C_2 Swan system and the arising atomic lines can be made. Beside that, a significant continuous blackbody emission is observed. Several explanations can be made for this appearance which is most likely due to the radiation of highly heated particles possibly injected into the flow field (e.g. by spallation) and as well observed at Raiche et al.[20] for PICA ablation.

In the following time dependent behaviour no specific characteristics are observed except for an overall decrease in intensity of all emitting features, what is most probably due to the recession of the sample.

5.3.3 MONA ablation spectra in air plasma

Examining spectra of the ablative sample in air atmosphere, more species have to be included since oxygen is available from the free-stream. Measurements are again taken ahead of the ablating sample. Figure 5-12 depicts spectra obtained for the same test conditions as shown above for N_2 but in air atmosphere. Again, plots are shown for each condition beginning with insertion of the sample and then proceeding in time. Comparing the upper image with the spectrum obtained for the air free-stream, now the higher emission of CN violet due to the injected sample is visible, but with much lower intensity (~10 times) than for the nitrogen test case whilst the CN red system is barely to identify. This smaller amount of CN in air is most likely due to the oxygen forming rather CO and CO_2 in an exothermic reaction with carbon than combining with nitrogen. Beside that and even more noticeable is the absence of molecular carbon during injection as identified before in nitrogen by means of the C_2 Swan system. Only for the higher heat flux case of 1.0MW/m² a small emission of C_2 Swan sequences could be identified but completely disappears after t=2s. Additionally, atomic transitions emerging from the ablation process are directly visible after insertion of the sample, contrary to nitrogen where it took several seconds for them to develop. However, up to this point the same atomic transitions are apparent for air and nitrogen.

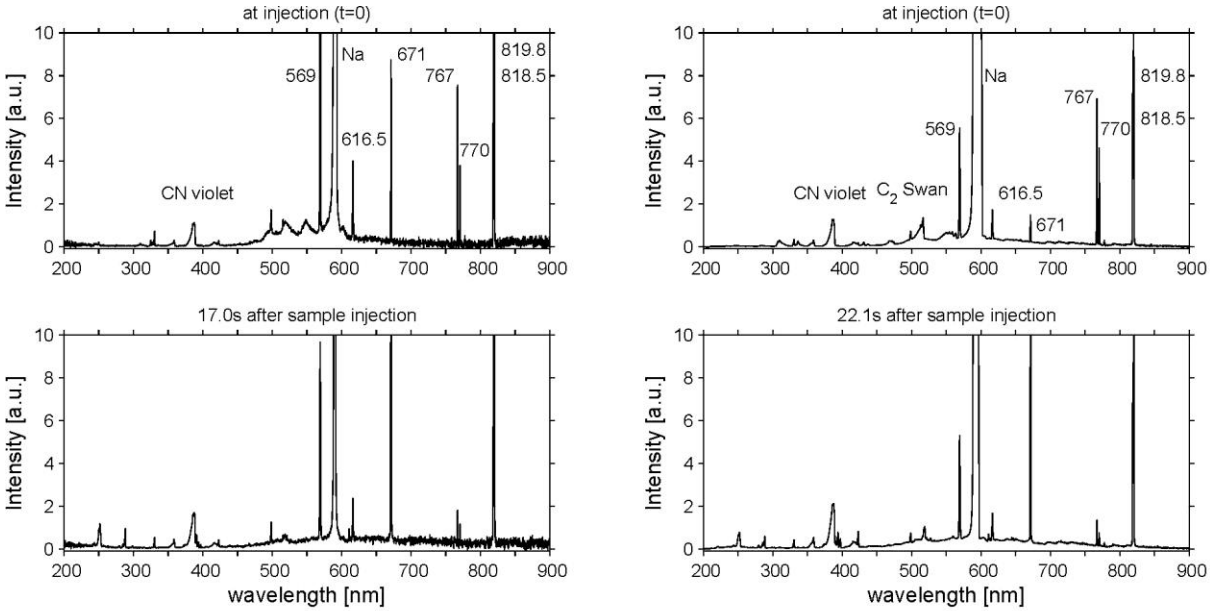

(a) 0.85MW/m² *(b) 1.0MW/m²*

Figure 5-12: Emission spectra ahead of the ablating MONA sample in air test gas at different times after injection for 0.85MW/m² (a) and 1.0MW/m² (b), 100mbar

Proceeding in time, the spectra for both heat fluxes presented in air do not change noticeably but decrease very fast in time, therefore, only one other point in time for each condition (t=17.0s for (a) and t=22.1s respectively for (b)) is shown. This is probably due to the recession of the surface, which is higher in air and hence, moving out of the fixed line of sight of the spectrometer. For other tests like No.A3 using a higher pressure, the continuous blackbody radiation appeared again.

5.3.4 Cork ablation spectra in air plasma

Further testing was performed using an ablator made up out of cork in a compound. Figure 5-13 depicts spectra obtained for different heat fluxes, being 1 & 3 MW/m², in air atmosphere. Plots are shown for each condition beginning with insertion of the sample and then proceeding in time. Comparing the upper image of Figure 5-13 (a) with the spectrum obtained for the air free-stream, now a higher emission of CN violet due to the injected sample is visible. This results in an emission of CN violet being around ten times higher than for the freestream due to ablation for both, 1 MW/m² and 3 MW/m² test case. Further, a higher amount of CN in nitrogen would be very likely due to the missing formation with oxygen, which leads rather to an exothermic reaction with carbon (CO) than combining with nitrogen (CN).

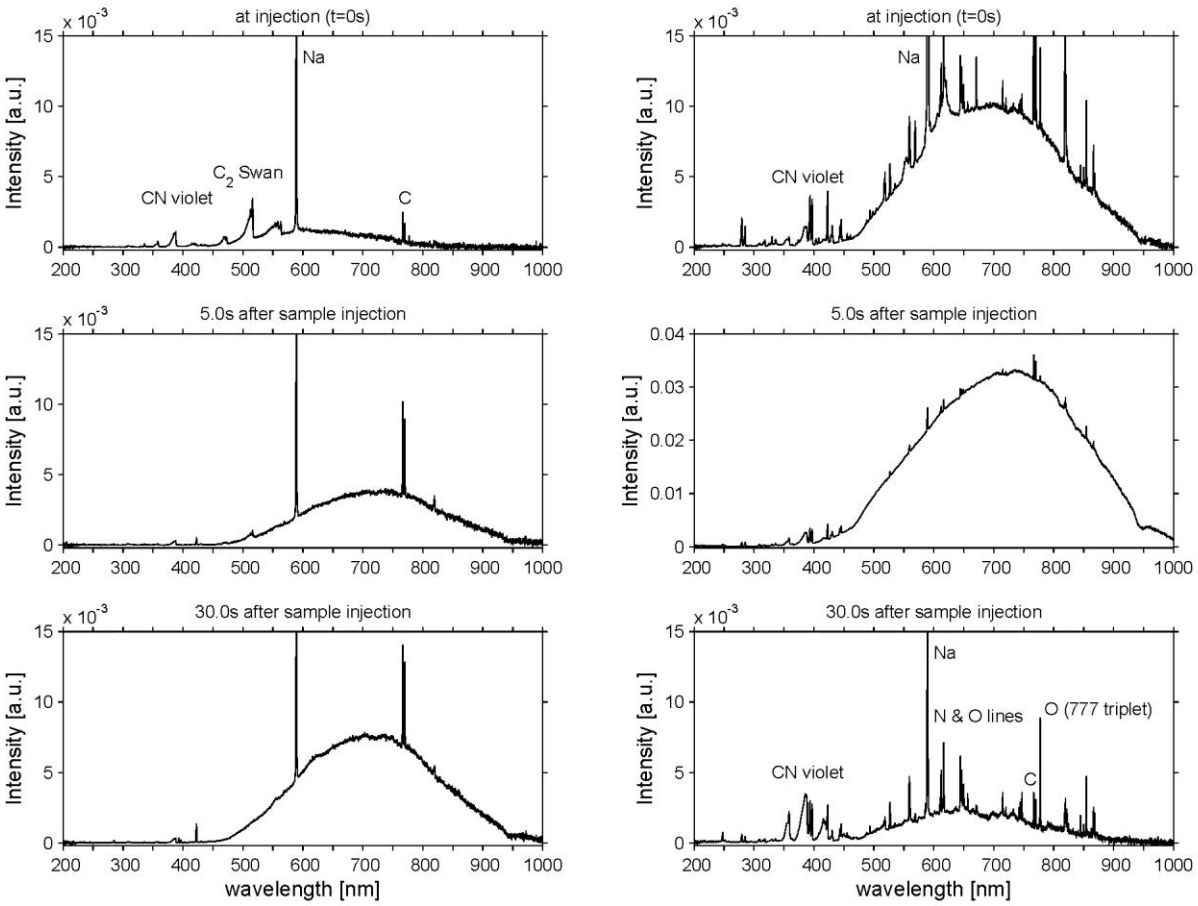

(a) 1.0 MW/m² ***(b) 3.0 MW/m²***

Figure 5-13: Emission spectra ahead of ablating cork sample in air test gas at different times after injection for different heat fluxes, p_s=100mbar

Beside that, amounts of C_2 (C_2 Swan) are obtained during the ablation test right after injection of the test sample into the plasma flow ((t=0s), Figure 5-13 (a) up). However, the amount of C_2 becomes much less after a few seconds within the ablation process (t=5s, Figure 5-13 (a) middle) and further, disappears completely until the end of the test (t=30s, Figure 5-13 (a) low). The very strong emitting line at 589 nm is most likely assignable to the sodium (Na) double rule at 588.99 nm and 589.59 nm, respectively, which are called D_1 and D_2 lines. Sodium might be one of the products comprised by the phenolic composition or could be due to impurities during the manufacturing process of the cork compound ablator. This highly radiating sodium line is present throughout all test cases. In addition, a significant continuous blackbody emission is observed with proceeding test time. Several explanations can be made for this appearance which is most likely due to the radiation of highly heated particles possibly injected into the flow field (e.g. by spallation) and as well observed at Raiche et al.[20] for PICA ablation.

Looking at the higher heat flux of 3 MW/m² used for ablation testing much more emitting transitions are visible in the recorded spectral range. Beside the still apparent CN molecule (CN violet), which has a higher concentration in this condition (higher intensity) atomic lines mostly arising from atomic oxygen and nitrogen are captured. Also, as for the lower heat flux case, a blackbody emission can be seen but directly developing at the injection of the sample. Possibilities for this high radiation with injection could either be due to a high burn-off rate as the sample ablates or a misalignment of the spectrometer, pointing directly on the sample instead of in front of it. With the proceeding in time this blackbody emission decreases and the various atomic lines are again visible (t=30s, Figure 5-13 (b)). With the heat flux being three times higher than for the other ablation test, the recession rate is increased. Hence, the surface of the ablating sample is moving out of the line of sight of the spectrometer, leading to a decrease in the collected emissions and therefore, the intensity levels.

6 CONCLUSION

The development of a multi-disciplinary experimental campaign was carried out at the Plasmatron facility of the von Karman Institute for the testing, analysis and qualification of ablative test samples. The results presented in this work demonstrated the successful application of a comprehensive experimental setup including intrusive and non-intrusive measurement techniques within ablation material testing. The ablator used throughout the campaign was an advanced, light-weight, composite based material (MONA) and a cork compound.

First tests were performed with graphite to ensure the functionality of each technique. The measurement of the front surface temperature of the ablative test samples by infrared thermography is a technique of major importance. Amorim P50 cork composite and MONA samples are tested at 1 MW/m^2 and 3 MW/m^2 heat flux conditions with air plasma at 100 bar static pressure. Other than type K thermocouples measuring the inner temperature of the test samples, a two-colour pyrometer, an infrared camera and a radiometer are used for temperature determination. The pyrometer can detect the most reliable surface temperature values as it is independent of the emissivity of the test material. However the pyrometer measurements lack the information of the emissivity of the material at test conditions and they are only valid above a certain temperature (1300 C for this case). The emissivity values for the two test cases are determined comparing the infrared camera and pyrometer data, as well as by comparing the radiometer values and the pyrometer measurements. The emissivity values obtained from the two methods agree well if one considers the transmissivity of the ZnSe window. The advantage of utilising an infrared camera is that it supplies spatially resolved thermal information, although it has higher noise level as can be observed in Figure 5-6 and Figure 5-7. On the other hand, although the radiometer supplies an averaged thermal response over a certain area (similar to the pyrometer), it provides low noise values.

Recession was measured by pre- and post-test sample evaluation (calliper rule) as well as in-situ using a high speed camera. This showed new promising results for the evaluation of recession speed during the test with applying post-test contour detection. Here, similar mass loss rates were measured for the samples independent of the used test gas whereas in an oxygen rich environment a much higher recession rate was observed. Whilst pyrolysis in-depth of the material is independent of oxygen, the ablation of the char layer was found to be mainly driven by oxidation leading to a high recession. The decomposition of the phenolic resin filler inside the material due to pyrolysis has a much higher contribution on mass loss

than the removal of mass caused by ablation of the outer thin char layer. Further, from the data available it was difficult to evaluate the degradation due to oxygen inside the sample, which could be a process restricted only to the surface or also appearing in-depth, speaking for a volumetric ablation. For this, cutting of the samples and microscopic examination would provide more information on the ability of oxygen to penetrate into depth by diffusion rather than being consumed by oxidation reactions at the surface.

With the measurements obtained from emission spectroscopy in front of the ablating MONA and cork sample, it was shown that nitridation leading to CN (CN violet, CN red) is highly apparent in pure nitrogen plasma flows but significantly drops when oxygen is involved, speaking for dominant oxidation reactions (CO, CO_2, NO).

Additionally, different chemical mechanisms were found to occur rather in nitrogen than in air plasma. In such a way, diatomic carbon (C_2 Swan) transitions were highly radiating after injection of the ablative sample into N_2 plasma but truncated after a few seconds. As expected, oxygen is the driving force to provoke reactions as the system undergoes the ablation process, but its uncertain state of diffusion into the porous material and on the contrary, reactions undergone in the absence of oxygen, call for more investigation.

7 RECOMMENDATIONS FOR FUTURE WORK

A lot of measurement techniques were applied in order to characterise the ablation process by combining intrusive and non-intrusive techniques based on different working principles. As this was a complex task, different recommendations have to be made on both, further ablation testing with a similar experimental setup and the processing of the data being (still) available.

- the HR4000 spectrometer used for the study was a very efficient, sufficiently resolving tool which, in particular, made it possible to capture time resolved ablation spectra. But due to the high interest in the influence of oxidation and the resulting radiation of NO and CO in the ultraviolet region, a change to a higher resolvable, more accurate spectrometer should also be done for air test cases.
- a mostly unpredictable uncertainty within the temperature measurements was introduced by the thermocouples being inserted into the test sample from the back, without any knowledge of the final position. Therefore it is recommended to perform X-ray examination of all tested samples to ensure a low error made for temperature measurements inside the sample.
- another problem regarding the data synchronisation of the thermocouples was the unknown injection time of the sample into the plasma flow. An approach was used, where a very small jump in the output of both thermocouples was measured instantly, assuming this is coming from the 'filling up' of the sample with hot gases. This approach was verified by subsequent tests. As this is only possible to be applied for porous material it is recommended to set a 'marker' manually at sample injection, which is displayed in the data output.
- regarding the analysis of the samples, which were tested in hot plasma flows, was only made so far by means of the measurement techniques introduced in this report. This does not give any view insight the sample and only assumptions on the inner state can be made. Therefore, cutting of the sample going along with microscopic examination would provide a lot of important additional information. Up to this point, this was planned to be performed

using the samples of the current test campaign, but without any results obtained so far.

- several tests were performed at different heat fluxes using different gases, exposing interesting results regarding the erosion, where discrepancies between mass loss and recession were found. To enforce this results and rather, to obtain more information, mainly regarding the diffusion and reaction of oxygen within the sample, more tests at other test conditions would be necessary. By doing so, further studies could be performed to address the question if rather surface or volumetric ablation is apparent.
- before injection, the sample is located just beside the hot plasma flow during the whole start-up procedure of the facility which can take up to several minutes. Therefore, it is already heated during this process what could also be seen at the thermocouple data. Hence, the design of a protective box is recommended to avoid this pre-heating and the effect on the sample going along with it.
- The utilization of a recession sensor is proposed for accurate measurements of the surface recession and to compare/validate results obtained by means of high speed camera imaging

- for in-situ recession analysis using a high speed camera a sensor with higher resolution can lead to a lower uncertainty arising from its conversion pixel:millimeter

Acknowledgements

Lockheed Martin UK is gratefully acknowledged for providing Carbon Resin Composite (MONA) ablator samples used in this study for ablation investigations. Besides, the Portuguese company AMORIM (AMORIM Cork Composites) is kindly thanked for enabling extensive testing of a cork-compound ablator by providing the needed bulk material.

REFERENCES

[1] Howe, J., Hypervelocity Atmospheric Flight: Real Gas Flow Fields, NASA TM 101055, 1989.

[2] Laub, B., and Venkatapathy, E., Thermal Protection and Facility Needs for *Demanding Future Planetary Missions*, International Workshop on Planetary Probe Atmospheric Entry and Descent Trajectory Analysis and Science, Lisbon, Portugal, October 6-9, 2003.

[3] Guthrie, J. D., Battat, B., and Severin, B. K., Thermal Protection Systems For Space Vehicles, Advanced Material and Processes Technology, Rome, NY.

[4] Chen, Y. K., and Milos F. S., Two-Dimensional Implicit Thermal Response and Ablation, Program for Charring Materials, Journal of Spacecraft and Rockets, Vol.38, No. 4, July August 2001.

[5] Gordeev, A. N., Overview of Characerisics and Experiments in IPM Plasmatrons, RTO AVT Course on "Measurement TEchniques for High Enthalpy and Plasma Flows", Belgium, October 25-29, 1999.

[6] Thömel J., et al, Sensitivity analysis of the Local Heat Transfer Simulation for the Application to Thermal Protection Systems, 9th AIAA/ASME Joint Thermophysics and Heat Transfer Conference, San Francisco (CA), USA, June 5-8, 2006.

[7] Gülhan, A., Application of Pyrometry and IR-Thermography to High Surface Temperature Measurements, RTO AVT Course on "Measurement Techniques for High Enthalpy and Plasma Flows", Belgium, October 25-29, 1999.

[8] Gülhan, A., *Heat Flux Measurements in High Enthalpy Flows*, RTO AVT Course on "Measurement Techniques for High Enthalpy and Plasma Flows", Belgium, October, 25-29, 1999.

[9] Kurtz, M. A., Diagnostic Tools for Plasma Wind Tunnels and Reentry Vehicles at the IRS, "Measurement Techniques for High Enthalpy and Plasma Flows", Belgium, October 25-29, 1999.

[10] Bottin, B., et al, The VKI Plasmatron Characteristics and Performance, RTO AVT Course on "Measurement Techniques for High Enthalpy and Plasma Flows", Belgium, October 25-29, 1999.

[11] Vancrayenest B., and Fletcher D. G., Investigation of the Thermochemistry of Ablation of Graphite for Planetary Entry Applications, 38th AIAA Thermophysics Conference Meeting and Exhibit, Ontorio, Canada June 6-9, 2005.

[12] Vancreyenest B. and Fletcher D.G., Emission Spectroscopic Survey of Graphite Ablation in the VKI Plasmatron, 9th AIAA/ASME Joint Thermophysics and Heat Transfer Conference, San Francisco USA, June 5-8, 2006.

[13] Yang K., Design of an Enhanced Probe Holder for High Heat Flux Measurements in Plasmatron, VKI Stagiare Report 2008-42, September 2008.

[14] Orsini, A., Nonequilibrium Vibrational Kinetics and Heat Transfer in the Boundary Layer of Axisymmetric Bodies Under Atmospheric Re-Entry Conditions, VKI Stagiaire Report 2005-23, June 2005.

[15] Kolesnikov, A. F., et al, Comparative Analysis of the Inductive Plasmatrons Capabilities for Thermochemical Simulation at the Earth and Mars Atmospheric Entry Conditions, ESA/ESTEC, Noordwijk, The Netherlands, 2002.

[16] Scala, S. M. and Gilbert, L.M., Sublimation of Graphite at Hypersonic Speeds, AIAA Journal, Vol.3, No.9, September 1965.

[17] Metzger, J. W., Engel, M. J., and Diaconis, N. S., Oxidation and Sublimation of Graphite in Simulated Re-entry Environments, AIAA Journal, Vol. 5, No. 3, March 1967.

[18] Abe, T., Overview of Research for Prediction of Aerodynamic Heating Environment During a Super-Orbital Reentry Flight of MUSES-C Reentry Capsule, The Institue of Space and Astronautical Science Report SP, Vol. No.17, March 2003.

[19] Paolucci, D., Design and Testing of Heat-flux Probe for Planetary Re-entry Condition Simulations, stagiaire Report 2006-07, Von Karman Institute for Fluid Dynamics, Rhode-Saint-Genese, Belgium.

[20] Raiche, G. A., Driver, D. M., Shock Layer Optical Attenuation and Emission Spectroscopy During Arc Jet Testing With Ablative Models, AIAA 42nd Aerospace Sciences Meeting & Exhibit , Reno, Nevada, 5-8 January 2004, AIAA2004-0825

[21] Martin W., Fuhr J., Kelleher D., Musgrove A., Sugar J. , Wiese W., et al., 1999, [Online] Available: http://www.nist.gov/index.html [June 2010], Gaithersburg, MD

[22] Ahn H.-K., Park C., Sawada K. Response of Heatshield Material at Stagnation Point of Pioneer-Venus Probes. Journal of thermophysics and heat transfer, Vol. 16, No.3:432-439, 2002

[23] Lachaud J., Cozmuta I., Mansour N. N.. Multiscale approach to ablation modeling of phenolic impregnated carbon ablators. Journal of Spacecraft and Rockets, accepted for publication, in the press.